Numerical and exact models for free vibration analysis of cylindrical and spherical shell panels

Numerical and exact models for free vibration analysis of cylindrical and spherical shell panels

F. Tornabene† , S. Brischetto‡*, N. Fantuzzi† and E. Viola†

† DICAM Department, University of Bologna

‡ Department of Mechanical and Aerospace Engineering, Politecnico di Torino, Torino, Italy

Abstract

The present paper shows a comparison between classical two-dimensional (2D) and three-dimensional (3D) finite elements (FEs), classical and refined 2D generalized differential quadrature (GDQ) methods and an exact three-dimensional solution. A free vibration analysis of one-layered and multilayered isotropic, composite and sandwich cylindrical and spherical shell panels is made. Low and high order frequencies are analyzed for thick and thin simply supported structures. Vibration modes are investigated to make a comparison between results obtained via the FE and GDQ methods (numerical solutions) and those obtained by means of the exact three-dimensional solution. The 3D exact solution is based on the differential equations of equilibrium written in general orthogonal curvilinear coordinates. This exact method is based on a layer-wise approach, the continuity of displacements and transverse shear/normal stresses is imposed at the interfaces between the layers of the structure. The geometry for shells is considered without any simplifications. The 3D and 2D finite element results are obtained by means of a well-known commercial FE code. Classical and refined 2D GDQ models are based on a generalized unified approach which considers both equivalent single layer and layer-wise theories. The differences between 2D and 3D FE solutions, classical and refined 2D GDQ models and 3D exact solutions depend on several parameters. These include the considered mode, the order of frequency, the thickness ratio of the structure, the geometry, the embedded material and the lamination sequence.

Keywords: analytical modelling; Computational modelling; Finite element analysis (FEA); Numerical analysis.

*Author for Correspondence: Salvatore Brischetto, Department of Mechanical and Aerospace Engineering, Politecnico di Torino, corso Duca degli Abruzzi, 24, 10129 Torino, ITALY. tel: +39.011.090.6813, fax: +39.011.090.6899, e.mail: salvatore.brischetto@polito.it.

1 Introduction

The present work proposes a free vibration analysis of simply-supported one-layered and multilayered isotropic, composite and sandwich cylindrical and spherical shell panels. Low and high frequencies and related modes are investigated. The importance of this topic has been extensively discussed in the reports by Leissa [1,2], in the book by Werner [3] and in the work by Brischetto and Carrera [4], among others.

The main aim of this work is the comparison between the results obtained by means of an exact three-dimensional (3D) solution, and those obtained by means of the classical two-dimensional (2D) and three-dimensional (3D) finite element methods (FEM) and by means of the classical and refined 2D generalized differential quadrature (GDQ) models. The proposed exact 3D solution was developed by Brischetto in [5–10] where the differential equations of equilibrium written in general orthogonal curvilinear coordinates were exactly solved by means of the exponential matrix method. The 2D and 3D FE results were obtained by means of the commercial finite element code Straus7 [11]. In this study, Straus7 was chosen for its user interface simplicity. In particular, it is easy to control the orientation of the plies in the stacking sequences and the location of the boundary conditions. The GDQ models were developed from the geometric description of the middle surface of shells. This description was carried out analytically using differential geometry [12,13]. The GDQ method can discretize any partial or total derivative using a weighted linear sum and the functional values in the definition domain. Therefore, it is easy and straightforward to transform the analytic description of a structure into a discrete set of equations [14–29]. The GDQ method was introduced by Shu and Richards [30] to solve physics problems related to fluids. A lot of advances have been made to date, which are summarized in the review papers [31–33]. It has been demonstrated that the GDQ method is a flexible and easy procedure for solving systems of partial differential equations in their strong form. Further applications related to finite elements in strong form using the GDQ method can be found in [34–40] in the case of vibrations of arbitrarily shaped structures.

In the most general case of exact three-dimensional analyses, the number of frequencies for a free vibration problem is infinite: three displacement components (3 degrees of freedom DOF) in each point (points are ∞ in the 3 directions x, y, z) leads to $3 \times \infty^3$ vibration modes. Assumptions are made in the thickness direction z in the case of a 2D plate/shell model, the three displacements in each point are expressed in terms of a given number of degrees of freedom (NDOF) through the thickness direction z. NDOF varies from theory to theory. As a result, the number of vibration modes is $NDOF \times \infty^2$ in the case of exact 2D models. For exact 1D beam models, the number of vibration modes is $NDOF \times \infty^1$. In the case of 2D computational models, such as the Finite Element (FE) method or the generalized differential quadrature (GDQ) models, the number of modes is a finite number. This number coincides with the total number of employed degrees of freedom: $\sum_1^{Node} NDOF_i$, where *Node* denotes the number of nodes used in the FE mathematical model or in the GDQ analysis, and $NDOF_i$ is the NDOF through the thickness direction z in the i-node. It is clear that some modes are not calculated by simplified models (such as computational two-dimensional models) [4]. In order to make a comparison between the 2D and 3D FE free vibration results, the 2D GDQ results, and the 3D exact free vibration results, the investigation of the vibration modes is mandatory in order to understand which frequencies must be compared.

The most relevant papers concerning 3D solutions for free vibration analysis of shell structures are shown below. The coupled free vibrations of a transversely isotropic cylindrical shell embedded in an elastic medium were analyzed in [41] where the three-dimensional elastic solution used three displacement functions. Free vibrations of simply-supported cylindrical shells were studied in [42] on the basis of three dimensional exact theory. Extensive frequency parameters were obtained by solving frequency equations. The free vibrations of simply-supported cross-ply cylindrical and doubly-curved laminates were investigated in [43]. The three-dimensional equations of motion were reduced

to a system of coupled ordinary differential equations and then solved using the power series method. The three-dimensional free vibrations of a homogenous isotropic, viscothermoelastic hollow sphere were studied in [44]. The surfaces were subjected to stress-free, thermally insulated or isothermal boundary conditions. The exact three-dimensional vibration analysis of a trans-radially isotropic, thermoelastic solid sphere was analyzed in [45]. The governing partial differential equations in [44] and [45] were transformed into a coupled system of ordinary differential equations. The Fröbenious matrix method was employed to obtain the solution. Soldatos and Ye [46] proposed exact, three-dimensional, free vibration analysis of angle-ply laminated thick cylinders with a regular symmetric or a regular antisymmetric angle-ply lay-up. Armenakas et al. [47] proposed a self-contained treatment of the problem of plane harmonic wave propagation along a hollow circular cylinder in the framework of the three-dimensional theory of elasticity. A comparison between a refined two-dimensional analysis, a shear deformation theory, the Flügge theory and an exact elasticity analysis was proposed in [48] for frequency investigation. Further details about the Flügge classical thin shell theory concerning the free vibrations of cylindrical shells with elastic boundary conditions can be found in [49]. Other comparisons between two-dimensional closed form solutions and exact 3D elastic analytical solutions for the free vibration analysis of simply supported and clamped homogenous isotropic circular cylindrical shells were also proposed in [50]. Vel [51] extended exact elasticity solutions to functionally graded cylindrical shells. The three-dimensional linear elastodynamic equations were solved using suitable displacement functions that identically satisfy the boundary conditions. Loy and Lam [52] obtained the governing equations using an energy minimization principle. A layer-wise approach was proposed to study the vibration of thick circular cylindrical shells on the basis of the three-dimensional theory of elasticity. Wang et al. [53] proposed a three-dimensional free vibration analysis of magneto-electro-elastic cylindrical panels. Further results about the three-dimensional analysis of shells, where the solutions are not given in closed form, can be found in [54] for the dynamic stiffness matrix method and in [55] and [56] for the three-dimensional Ritz method for the vibration of spherical shells.

Conical shells were parametrically investigated using the GDQ method in the works [57–59]. Free vibrations of spherical and other revolution shells were proposed in [25–29, 60–66]. Doubly-curved composite shells including new physical effects were proposed in the papers [14–22]. Each of the previous citations was fundamental for the present GDQ model because the code had been previously tested for different cases.

The three-dimensional analyses proposed in the literature show free vibrations of plates or shells. They separately analyze shell or plate geometries and they do not give a general overview for both structures. The proposed exact 3D model uses a general formulation for several geometries (square and rectangular plates, cylindrical and spherical shell panels, and cylindrical closed shells). The equations of motion for the dynamic case are written in general orthogonal curvilinear coordinates using an exact geometry for multilayered shells. The system of second order differential equations is reduced to a system of first order differential equations, and subsequently solved exactly using the exponential matrix method and the Navier-type solution. The approach is developed in a layer-wise form imposing the continuity of displacements and transverse shear/normal stresses at each interface. The exponential matrix method was already used in [67] for the three-dimensional analysis of plates in rectilinear orthogonal coordinates and in [46] for an exact, three-dimensional, free vibration analysis of angle-ply laminated cylinders in cylindrical coordinates. The equations of motion written in orthogonal curvilinear coordinates are a general form of the equations of motion written in rectilinear orthogonal coordinates in [67] and in cylindrical coordinates in [46]. The present 3D equations allow general exact solutions for multilayered plate and shell geometries as already seen in the second author's works [5–10]. In the literature review proposed in this introduction, only a few works analyzed higher order frequencies. Moreover, papers that discuss the comparison between numerical 2D models and exact 3D models are even less frequent. The present work aims to fill this gap, it compares the free frequencies for cylindrical and spherical shell panels obtained by means of the commercial FE code

Straus7, the 2D GDQ models, and the exact 3D solution. The proposed 3D exact solution gives results for plates, cylindrical and spherical shell panels, and cylindrical closed shells. However, the comparison with the commercial FE code and the GDQ models is proposed only for cylindrical and spherical shell panels because the plate and cylinder cases were already investigated in [8]. The aim of the present paper is to understand how to compare these three different methods (exact 3D and numerical FE and GDQ solutions) and also to show the limitations of classical 2D theories.

2 Exact three-dimensional model

The equations of equilibrium written for the case of free vibration analysis of multilayered spherical shells embedding N_L layers with constant radii of curvature R_α and R_β are (the general form for variable radii of curvature can be found in [68] and [12])

$$H_\beta \frac{\partial \sigma^k_{\alpha\alpha}}{\partial \alpha} + H_\alpha \frac{\partial \sigma^k_{\alpha\beta}}{\partial \beta} + H_\alpha H_\beta \frac{\partial \sigma^k_{\alpha z}}{\partial z} + \left(\frac{2H_\beta}{R_\alpha} + \frac{H_\alpha}{R_\beta} \right) \sigma^k_{\alpha z} = \rho^k H_\alpha H_\beta \ddot{u}^k \tag{1}$$

$$H_\beta \frac{\partial \sigma^k_{\alpha\beta}}{\partial \alpha} + H_\alpha \frac{\partial \sigma^k_{\beta\beta}}{\partial \beta} + H_\alpha H_\beta \frac{\partial \sigma^k_{\beta z}}{\partial z} + \left(\frac{2H_\alpha}{R_\beta} + \frac{H_\beta}{R_\alpha} \right) \sigma^k_{\beta z} = \rho^k H_\alpha H_\beta \ddot{v}^k \tag{2}$$

$$\begin{aligned} &H_\beta \frac{\partial \sigma^k_{\alpha z}}{\partial \alpha} + H_\alpha \frac{\partial \sigma^k_{\beta z}}{\partial \beta} + H_\alpha H_\beta \frac{\partial \sigma^k_{zz}}{\partial z} - \frac{H_\beta}{R_\alpha} \sigma^k_{\alpha\alpha} - \frac{H_\alpha}{R_\beta} \sigma^k_{\beta\beta} \\ &+ \left(\frac{H_\beta}{R_\alpha} + \frac{H_\alpha}{R_\beta} \right) \sigma^k_{zz} = \rho^k H_\alpha H_\beta \ddot{w}^k \end{aligned} \tag{3}$$

where ρ^k is the mass density, ($\sigma^k_{\alpha\alpha}$, $\sigma^k_{\beta\beta}$, σ^k_{zz}, $\sigma^k_{\beta z}$, $\sigma^k_{\alpha z}$, $\sigma^k_{\alpha\beta}$) are the six stress components and $\ddot{u}^k$, $\ddot{v}^k$ and $\ddot{w}^k$ indicate the second temporal derivative of the three displacement components. Each quantity depends on the k layer. R_α and R_β are referred to the mid-surface Ω_0 of the whole multilayered shell (see Figure 1 for further details about shell geometry). H_α and H_β continuously vary through the thickness of the multilayered shell and they depend on the thickness coordinate. The parametric coefficients for shells with constant radii of curvature are:

$$H_\alpha = \left(1 + \frac{z}{R_\alpha} \right) = \left(1 + \frac{\tilde{z} - h/2}{R_\alpha} \right) \quad H_\beta = \left(1 + \frac{z}{R_\beta} \right) = \left(1 + \frac{\tilde{z} - h/2}{R_\beta} \right) \quad H_z = 1 \tag{4}$$

H_α and H_β depend on z or $\tilde{z}$ coordinate (see Figure 2 for further details).

Geometrical relations link strains with displacements. Constitutive equations link stresses with strains. These two sets within the harmonic form for the displacement components can be substituted in equilibrium equations (1)-(3) in order to obtain the system of equations in closed form (further details can be found in [5–10])

$$\Big(-\frac{C_{55}^k H_\beta}{H_\alpha R_\alpha^2} - \frac{C_{55}^k}{R_\alpha R_\beta} - \bar{\alpha}^2 \frac{C_{11}^k H_\beta}{H_\alpha} - \bar{\beta}^2 \frac{C_{66}^k H_\alpha}{H_\beta} + \rho^k H_\alpha H_\beta \omega^2 \Big) U^k + \Big(-\bar{\alpha}\bar{\beta} C_{12}^k - \bar{\alpha}\bar{\beta} C_{66}^k \Big) V^k +$$
$$\Big(\bar{\alpha} \frac{C_{11}^k H_\beta}{H_\alpha R_\alpha} + \bar{\alpha} \frac{C_{12}^k}{R_\beta} + \bar{\alpha} \frac{C_{55}^k H_\beta}{H_\alpha R_\alpha} + \bar{\alpha} \frac{C_{55}^k}{R_\beta} \Big) W^k + \Big(\frac{C_{55}^k H_\beta}{R_\alpha} + \frac{C_{55}^k H_\alpha}{R_\beta} \Big) U_{,z}^k + \Big(\bar{\alpha} C_{13}^k H_\beta + \tag{5}$$
$$\bar{\alpha} C_{55}^k H_\beta \Big) W_{,z}^k + \Big(C_{55}^k H_\alpha H_\beta \Big) U_{,zz}^k = 0$$
$$\Big(-\bar{\alpha}\bar{\beta} C_{66}^k - \bar{\alpha}\bar{\beta} C_{12}^k \Big) U^k + \Big(-\frac{C_{44}^k H_\alpha}{H_\beta R_\beta^2} - \frac{C_{44}^k}{R_\alpha R_\beta} - \bar{\alpha}^2 \frac{C_{66}^k H_\beta}{H_\alpha} - \bar{\beta}^2 \frac{C_{22}^k H_\alpha}{H_\beta} + \rho^k H_\alpha H_\beta \omega^2 \Big) V^k +$$
$$\Big(\bar{\beta} \frac{C_{44}^k H_\alpha}{H_\beta R_\beta} + \bar{\beta} \frac{C_{44}^k}{R_\alpha} + \bar{\beta} \frac{C_{22}^k H_\alpha}{H_\beta R_\beta} + \bar{\beta} \frac{C_{12}^k}{R_\alpha} \Big) W^k + \Big(\frac{C_{44}^k H_\alpha}{R_\beta} + \frac{C_{44}^k H_\beta}{R_\alpha} \Big) V_{,z}^k + \Big(\bar{\beta} C_{44}^k H_\alpha + \tag{6}$$
$$\bar{\beta} C_{23}^k H_\alpha \Big) W_{,z}^k + \Big(C_{44}^k H_\alpha H_\beta \Big) V_{,zz}^k = 0$$
$$\Big(\bar{\alpha} \frac{C_{55}^k H_\beta}{H_\alpha R_\alpha} - \bar{\alpha} \frac{C_{13}^k}{R_\beta} + \bar{\alpha} \frac{C_{11}^k H_\beta}{H_\alpha R_\alpha} + \bar{\alpha} \frac{C_{12}^k}{R_\beta} \Big) U^k + \Big(\bar{\beta} \frac{C_{44}^k H_\alpha}{H_\beta R_\beta} - \bar{\beta} \frac{C_{23}^k}{R_\alpha} + \bar{\beta} \frac{C_{22}^k H_\alpha}{H_\beta R_\beta} + \bar{\beta} \frac{C_{12}^k}{R_\alpha} \Big) V^k +$$
$$\Big(\frac{C_{13}^k}{R_\alpha R_\beta} + \frac{C_{23}^k}{R_\alpha R_\beta} - \frac{C_{11}^k H_\beta}{H_\alpha R_\alpha^2} - \frac{2 C_{12}^k}{R_\alpha R_\beta} - \frac{C_{22}^k H_\alpha}{H_\beta R_\beta^2} - \bar{\alpha}^2 \frac{C_{55}^k H_\beta}{H_\alpha} - \bar{\beta}^2 \frac{C_{44}^k H_\alpha}{H_\beta} + \rho^k H_\alpha H_\beta \omega^2 \Big) W^k + \tag{7}$$
$$\Big(-\bar{\alpha} C_{55}^k H_\beta - \bar{\alpha} C_{13}^k H_\beta \Big) U_{,z}^k + \Big(-\bar{\beta} C_{44}^k H_\alpha - \bar{\beta} C_{23}^k H_\alpha \Big) V_{,z}^k + \Big(\frac{C_{33}^k H_\beta}{R_\alpha} + \frac{C_{33}^k H_\alpha}{R_\beta} \Big) W_{,z}^k +$$
$$\Big(C_{33}^k H_\alpha H_\beta \Big) W_{,zz}^k = 0$$

The system of second order differential equations proposed in Eqs.(5)-(7) can be reduced to a system of first order differential equations using the method described in [69] and [70] (further details can also be found in [5–10])

$$\begin{bmatrix} A_6^k & 0 & 0 & 0 & 0 & 0 \\ 0 & A_{12}^k & 0 & 0 & 0 & 0 \\ 0 & 0 & A_{19}^k & 0 & 0 & 0 \\ 0 & 0 & 0 & A_6^k & 0 & 0 \\ 0 & 0 & 0 & 0 & A_{12}^k & 0 \\ 0 & 0 & 0 & 0 & 0 & A_{19}^k \end{bmatrix} \begin{bmatrix} U^k \\ V^k \\ W^k \\ U^{k\prime} \\ V^{k\prime} \\ W^{k\prime} \end{bmatrix}' = \begin{bmatrix} 0 & 0 & 0 & A_6^k & 0 & 0 \\ 0 & 0 & 0 & 0 & A_{12}^k & 0 \\ 0 & 0 & 0 & 0 & 0 & A_{19}^k \\ -A_1^k & -A_2^k & -A_3^k & -A_4^k & 0 & -A_5^k \\ -A_7^k & -A_8^k & -A_9^k & 0 & -A_{10}^k & -A_{11}^k \\ -A_{13}^k & -A_{14}^k & -A_{15}^k & -A_{16}^k & -A_{17}^k & -A_{18}^k \end{bmatrix} \begin{bmatrix} U^k \\ V^k \\ W^k \\ U^{k\prime} \\ V^{k\prime} \\ W^{k\prime} \end{bmatrix} \tag{8}$$

Eq.(8) can be written in a compact form for a generic k layer

$$\boldsymbol{D}^k \frac{\partial \boldsymbol{U}^k}{\partial \tilde{z}} = \boldsymbol{A}^k \boldsymbol{U}^k \tag{9}$$

where $\frac{\partial \boldsymbol{U}^k}{\partial \tilde{z}} = \boldsymbol{U}^{k\prime}$ and $\boldsymbol{U}^k = [U^k\ V^k\ W^k\ U^{k\prime}\ V^{k\prime}\ W^{k\prime}]$. The meaning of coefficients A_s^k with s from 1 to 19 is indicated in each block $\Big(\Big)$ of Eqs.(5)-(7).

In the case of plate geometry coefficients A_3^k, A_4^k, A_9^k, A_{10}^k, A_{13}^k, A_{14}^k and A_{18}^k are zero because the radii of curvature R_α and R_β are infinite. The other coefficients A_1^k, A_2^k, A_5^k, A_6^k, A_7^k, A_8^k, A_{11}^k, A_{12}^k, A_{15}^k, A_{16}^k, A_{17}^k and A_{19}^k are constant in each k layer because parametric coefficients $H_\alpha = H_\beta = 1$ and they do not depend on the thickness coordinate $\tilde{z}$. Therefore, matrices $\boldsymbol{D}^k$ and $\boldsymbol{A}^k$ are constant in each k layer of the plate. In the case of shell geometry coefficients A_s^k are not constant and they depend on the thickness coordinate z. For plate geometry the differential equations of equilibrium can be solved by means of the exponential matrix method (see [70], [71] and [72]), because they have constant

coefficients. Shell geometries have differential equations with variable coefficients (they depend on the z coordinate) and they can be solved applying the exponential matrix method in several fictitious layers j which have been introduced to calculate the parametric coefficients $H_\alpha(z)$ and $H_\beta(z)$.

In order to obtain the multilayer matrix $\boldsymbol{E}$ for plates and shells, $N_L - 1$ transfer matrices $\boldsymbol{T}^{k-1,k}$ must be calculated using for each interface the following conditions for interlaminar continuity of displacements and transverse shear/normal stresses

$$u_b^k = u_t^{k-1}\,,\;\; v_b^k = v_t^{k-1}\,,\;\; w_b^k = w_t^{k-1} \tag{10}$$

$$\sigma_{zzb}^k = \sigma_{zzt}^{k-1}\,,\;\; \sigma_{\alpha zb}^k = \sigma_{\alpha zt}^{k-1}\,,\;\; \sigma_{\beta zb}^k = \sigma_{\beta zt}^{k-1} \tag{11}$$

each displacement and transverse stress component at the top (t) of the k-1 layer is equal to displacement and transverse stress components at the bottom (b) of the k layer. Moreover, the structures are simply supported and free stresses at the top and at the bottom of the whole multilayered shell, this feature means

$$\sigma_{zz} = \sigma_{\alpha z} = \sigma_{\beta z} = 0 \quad \text{for} \quad z = -h/2, +h/2 \quad \text{or} \quad \tilde{z} = 0, h \tag{12}$$

$$w = v = 0,\; \sigma_{\alpha\alpha} = 0 \quad \text{for} \quad \alpha = 0, a \tag{13}$$

$$w = u = 0,\; \sigma_{\beta\beta} = 0 \quad \text{for} \quad \beta = 0, b \tag{14}$$

Using Eqs.(10)-(11) and (12)-(14), the following system is obtained (further details can be found in [5–10])

$$\boldsymbol{E} \quad \boldsymbol{U}_1(0) \;=\; \boldsymbol{0} \tag{15}$$

where $\boldsymbol{U}_1(0)$ is the displacement vector at the bottom of the first layer and $\boldsymbol{E}$ is the 6×6 multilayer matrix that is valid for plates and shells (in this last case fictitious layers j have been introduced for the solution). Matrix $\boldsymbol{E}$ has always 6×6 dimension, independently from the number of layers, even if the method uses a layer-wise approach. The solution is implemented in a Matlab code where only the spherical shell method is considered, it automatically degenerates into cylindrical open/closed shell and plate geometries.

The free vibration analysis means to find the non-trivial solution of $\boldsymbol{U}_1(0)$ in Eq.(15), this means to impose the determinant of matrix $\boldsymbol{E}$ equals zero:

$$\det[\boldsymbol{E}] = 0 \tag{16}$$

Eq.(16) means to find the roots of a higher order polynomial in $\lambda = \omega^2$. For each pair of half-wave numbers (m, n) a certain number of circular frequencies are obtained depending on the order N chosen for each exponential matrix.

A certain number of circular frequencies ω_l are found when half-wave numbers m and n are imposed in the structures. For each frequency ω_l, it is possible to find the vibration mode through the thickness in terms of the three displacement components. If the frequency ω_l is substituted in the 6×6 matrix $\boldsymbol{E}$, this last matrix has six eigenvalues. We are interested to the null space of matrix $\boldsymbol{E}$ that means to find the 6×1 eigenvector related to the minimum of the six eigenvalues proposed. This null space is, for the chosen frequency ω_l, the vector $\boldsymbol{U}$ calculated at the bottom of the whole structure

$$\boldsymbol{U}_{1\omega_l}(0) = \left[\; U_1(0) \quad V_1(0) \quad W_1(0) \quad U_1'(0) \quad V_1'(0) \quad W_1'(0) \;\right]_{\omega_l}^T \tag{17}$$

T means the transpose of the vector and the subscript ω_l means that the null space is calculated for the circular frequency ω_l.

It is possible to find $\boldsymbol{U}_{q\omega_l}(\tilde{z}_q)$ (with the three displacement components $U_{q\omega_l}(\tilde{z}_q)$, $V_{q\omega_l}(\tilde{z}_q)$ and $W_{q\omega_l}(\tilde{z}_q)$ through the thickness) for each q layer of the multilayered structure with the index $q = k \times j$ (in place of k) from 1 to P. The thickness coordinate $\tilde{z}$ can assume all the values from the bottom to the top of the structure. For the plate case the procedure is simpler because there are not the j fictitious layers and the index $q = k \times j$ coincides with the index k of the physical layers (in this case, the total number of layers is N_L and it is not P).

2.1 Validation of the 3D exact model

Before the comparison study between the 3D exact solution and the several 2D numerical methods, the proposed 3D exact model has been validated by means of several comparisons with other 3D results already given in the literature. The validation considers cylindrical panels and spherical panels (see Figure 3 for further details). The order of expansion employed for the exponential matrix is $N = 3$. $P = 100$ fictitious layers will always be used for the proposed assessments and benchmarks. $P = 102$ fictitious layers will be used only for the investigation of three-layered structures. An appropriate convergence study was already proposed in [5–7].

The first assessment gives several frequencies for a simply supported multilayered composite cylindrical panel with radii of curvature $R_\alpha = 10$ m and $R_\beta = \infty$, and dimensions $a = b = 5$ m. The thickness is $h = 0.5$ m (the shell is moderately thick with a thickness ratio $R_\alpha/h = 20$). The composite layers have properties $E_1 = 25E_0$, $E_2 = E_3 = E_0$, $G_{12} = G_{13} = 0.5E_0$, $G_{23} = 0.2E_0$, $\nu_{12} = \nu_{13} = \nu_{23} = 0.25$ and $\rho = 1500$ kg/m^3. Non-dimensional circular frequencies $\bar{\omega} = \omega R_\alpha \sqrt{\frac{\rho}{E_0}}$ for several physical layers N_L and lamination sequence $(0°/90°/0°/90°/\ldots)$ are given in Table 1. The imposed half-wave numbers m and n are indicated in the table. For $m = n = 1$ the first three modes (I,II and III) are shown, only the first mode (I) is given for the other combinations of half-wave numbers m and n. The present 3D solution is coincident with the 3D solution by Huang [43] for each proposed half-wave number, vibration mode, and number of physical layers N_L embedded in the multilayered composite structure.

The second assessment considers several frequencies for a simply supported multilayered composite spherical panel with radii of curvature $R_\alpha = 10$ m and $R_\beta = 10$ m, dimensions $a = b = 2$ m and thickness value $h = 0.2$ m (the shell is moderately thin with a thickness ratio $R_\alpha/h = 50$). The composite layers have the same properties already seen for the first assessment. Non-dimensional circular frequencies $\bar{\omega} = \omega R_\alpha \sqrt{\frac{\rho}{E_0}}$ for several physical layers N_L and lamination sequence $(0°/90°/0°/90°/\ldots)$ are given in Table 2. The present 3D solution gives the same results of the 3D solution by Huang [43] for each proposed half-wave number and for each number of physical layers N_L embedded in the multilayered composite structure. The first vibration mode (I) is investigated for each combination of half-wave numbers m and n.

The proposed 3D solution was successfully validated for cylindrical and spherical shell panels. Several lamination sequences, thickness ratios, vibration modes and imposed half-wave numbers have been investigated. Therefore, the 3D model can be used with confidence to validate the numerical models and also to make the comparisons between the exact 3D results and the computational models.

3 2D and 3D finite element models

Straus7 (internationally known as Strand7) is a fully-integrated visual environment combined with a suite of powerful solvers. Straus7 implements different types of elements, but for the present applications 4-node (QUAD4) 2D elements and 20-node (HEXA20) 3D bricks have been considered. The previous published benchmarks regarding 2D FEs and 3D FEs [14–18,20,22,25–29,40,59–66] demonstrated that GDQ and FE methods are very similar, in particular for the vibration problems.

QUAD4 and HEXA20 are good choices for this type of analysis, even if other types of element can

be used. A review of the validations and comparisons between the Straus7 FE models and the GDQ method can be found in the books [12, 13].

3.1 Validation of the finite element models

Before the comparison study with the 3D exact solution, FE numerical benchmarks are proposed to show the convergence of the present FE code. Dashed lines in Figure 4 indicate the convergence for an isotropic and a laminated composite cylindrical panel. The isotropic material has $E = 73$ GPa, $\nu = 0.3$ and $\rho = 2800$ kg/m^3 (with $R_\alpha/h = 1000$ and $h = 0.01$ m). The lamination for the composite structure is $(90°/0°/90°/0°)$ and the orthotropic plies have $E_1 = 132.38$ GPa and $E_2 = E_3 = 10.756$ GPa, shear modulii $G_{12} = G_{13} = 5.6537$ GPa and $G_{23} = 3.603$ GPa, Poisson ratios $\nu_{12} = \nu_{13} = 0.24$ and $\nu_{23} = 0.49$, and mass density $\rho = 1600$ kg/m^3. The geometric properties of the panel are $R_\alpha = 10$ m, $b = 20$ m and $a = \frac{\pi}{3}R_\alpha$. Four QUAD4 meshes are taken into account dividing the geometry in 8×8, 16×16, 32×32, 64×64 elements. In the abscissa of Figure 4 the $\log_{10} I_N$ is given, I_N is the number of nodes along the side of the panel, e.g. $I_N = 9$, 17, 33, 65. It can be noted that increasing the number of elements for side the first ten frequencies are numerically stable. For the 3D FE analysis the same 64×64 in-plane mesh used for the 2D FE analysis is considered. Three elements per layer are taken into account according to what has been observed by the authors in their past works [13]- [18]. In particular, it has been observed that at least three quadratic elements should be used through the thickness per each layer in order to get accurate FEM results for such structures.

4 Refined 2D shell theories: equivalent single layer and layer wise procedures

Two refined 2D shell models are taken into account: an equivalent single layer and a layer-wise approach [77]. The first model considers a displacement field as

$$\mathbf{U} = \sum_{\tau=0}^{N_c+1} \mathbf{F}_\tau \mathbf{u}^{(\tau)} \tag{18}$$

where $\mathbf{U}$ indicates the 3D displacement component vector and $\mathbf{u}$ stands for the vector of the τth generalized displacements of the points in the middle surface of the shell [20]. $\mathbf{F}_{\tau(ij)} = \delta_{ij} F_\tau$, for $i, j = 1, 2, 3$ is the thickness function matrix and δ is the Kronecker delta function. In the present study two ESL models are shown: a first order model (the classic Reissner-Mindlin approach GDQ-RM for $N_c = 0$) and a higher-order model with an expansion order $N_c = 4$ and the optional Murakami's function (GDQ-ESL or GDQ-ZZ) [73]- [76]. Single layered structures do not have the ZZ function by definition [77].

The 3D strains, using an orthogonal co-ordinate system, can be defined as

$$\boldsymbol{\varepsilon} = \mathbf{D}\mathbf{U} = \mathbf{D}_Z \mathbf{D}_\Omega \mathbf{U} \tag{19}$$

where $\mathbf{D}_Z$, $\mathbf{D}_\Omega$ can be found in explicit form in [20] and $\boldsymbol{\varepsilon}$ is the strain component vector. Substituting the displacement field (18) into the strain-displacement relations (19) the following generalized terms are carried out

$$\boldsymbol{\varepsilon} = \sum_{\tau=0}^{N_c+1} \mathbf{D}_Z \mathbf{D}_\Omega \mathbf{F}_\tau \mathbf{u}^{(\tau)} = \sum_{\tau=0}^{N_c+1} \mathbf{Z}^{(\tau)} \mathbf{D}_\Omega \mathbf{u}^{(\tau)} = \sum_{\tau=0}^{N_c+1} \mathbf{Z}^{(\tau)} \boldsymbol{\varepsilon}^{(\tau)} \tag{20}$$

where $\boldsymbol{\varepsilon}^{(\tau)}$ is the τth order generalized strain component vector. The matrix $\mathbf{Z}^{(\tau)}$ contains only the geometric quantities through the shell thickness and it was presented in extended form in [20]. From (20) the relation between generalized strains $\boldsymbol{\varepsilon}^{(\tau)}$ and displacements $\mathbf{u}^{(\tau)}$ was found

$$\boldsymbol{\varepsilon}^{(\tau)} = \mathbf{D}_{\Omega}\mathbf{u}^{(\tau)} \quad \text{for} \quad \tau = 0, 1, 2, \ldots, N_c, N_c + 1 \tag{21}$$

The constitutive equations are referred to a general kth lamina by the well-known Hooke's law

$$\boldsymbol{\sigma}^{(k)} = \bar{\mathbf{C}}^{(k)}\boldsymbol{\varepsilon}^{(k)} \tag{22}$$

where $\boldsymbol{\sigma}^{(k)}$ is the stress component vector and $\bar{\mathbf{C}}^{(k)}$ the constitutive matrix for the kth ply [20]. The components of the constitutive matrix are indicated as $\bar{E}^{(k)}_{\xi\eta}$ and are referred to a curvilinear reference system $O'\alpha\beta z$ after the application of the transformation equations [20]. If a first order theory is considered these elastic coefficients have to be taken in their reduced form $\bar{E}^{(k)}_{\xi\eta} = \bar{Q}^{(k)}_{\xi\eta}$. In a higher-order model with the four-order of expansion, they have a non-reduced form $\bar{E}^{(k)}_{\xi\eta} = \bar{C}^{(k)}_{\xi\eta}$. This is important because first order theory neglects the stretching effect along the shell thickness, whereas the other higher-order model considers it (see also [78] and [79] for further details).

The internal actions or resultants of the τth order are derived from the Hamilton's Principle for a 3D doubly-curved solid [20]. It can be defined as

$$\mathbf{S}^{(\tau)} = \sum_{k=1}^{N_L} \int_{z_k}^{z_{k+1}} \left(\mathbf{Z}^{(\tau)}\right)^T \boldsymbol{\sigma}^{(\tau)} H_\alpha H_\beta dz \quad \text{for} \quad \tau = 0, 1, 2, \ldots, N_c, N_c + 1 \tag{23}$$

where $\mathbf{S}^{(\tau)}$ is the τth order internal action vector. The τth order resultants in terms of generalized sth order strains $\boldsymbol{\varepsilon}^{(s)}$ can be defined by using the equations (20)-(23)

$$\mathbf{S}^{(\tau)} = \sum_{s=0}^{N_c+1} \mathbf{A}^{(\tau s)}\boldsymbol{\varepsilon}^{(s)} \quad \text{for} \quad \tau = 0, 1, 2, \ldots, N_c, N_c + 1 \tag{24}$$

where

$$\mathbf{A}^{(\tau s)} = \sum_{k=1}^{N_L} \int_{z_k}^{z_{k+1}} \left(\mathbf{Z}^{(\tau)}\right)^T \bar{\mathbf{C}}^{(k)} \mathbf{Z}^{(s)} H_\alpha H_\beta dz \tag{25}$$

The elastic coefficients of the constitutive matrix (25), also reported in extended form in [20], explicitly assume the following form

$$\begin{aligned}
A^{(\tau s)}_{\xi\eta(\varrho\zeta)} &= \sum_{k=1}^{N_L} \int_{z_k}^{z_{k+1}} \bar{B}^{(k)}_{\xi\eta} F_s F_\tau \frac{H_\alpha H_\beta}{H^\varrho_\alpha H^\zeta_\beta} dz \\
A^{(\tilde{\tau} s)}_{\xi\eta(\varrho\zeta)} &= \sum_{k=1}^{N_L} \int_{z_k}^{z_{k+1}} \bar{B}^{(k)}_{\xi\eta} F_s \frac{\partial F_\tau}{\partial z} \frac{H_\alpha H_\beta}{H^\varrho_\alpha H^\zeta_\beta} dz \qquad \text{for} \quad \tau, s = 0, 1, 2, \ldots, N_c, N_c + 1 \\
A^{(\tau \tilde{s})}_{\xi\eta(\varrho\zeta)} &= \sum_{k=1}^{N_L} \int_{z_k}^{z_{k+1}} \bar{B}^{(k)}_{\xi\eta} \frac{\partial F_s}{\partial z} F_\tau \frac{H_\alpha H_\beta}{H^\varrho_\alpha H^\zeta_\beta} dz \qquad \text{for} \quad \xi, \eta = 1, 2, 3, 4, 5, 6 \\
A^{(\tilde{\tau} \tilde{s})}_{\xi\eta(\varrho\zeta)} &= \sum_{k=1}^{N_L} \int_{z_k}^{z_{k+1}} \bar{B}^{(k)}_{\xi\eta} \frac{\partial F_s}{\partial z} \frac{\partial F_\tau}{\partial z} \frac{H_\alpha H_\beta}{H^\varrho_\alpha H^\zeta_\beta} dz \qquad \text{for} \quad \varrho, \zeta = 0, 1, 2
\end{aligned} \tag{26}$$

with

$$\bar{B}_{\xi\eta}^{(k)} = \begin{cases} \bar{E}_{\xi\eta}^{(k)} & \text{for} \quad \xi,\eta = 1,2,3,6 \\ \kappa(z)\bar{E}_{\xi\eta}^{(k)} & \text{for} \quad \xi,\eta = 4,5 \end{cases} \tag{27}$$

where τ and s indicate the corresponding thickness function F_τ and F_s. In the present paper, F_τ and F_s have the classic power of z form for classic higher-order theories. For instance F_τ, $F_s = 1$, z, z^2, z^3, z^4, ..., z^{N_c}. It is recalled that the exponent $N_c + 1$ is reserved for the Murakami's function. The subscripts $\tilde{\tau}$, $\tilde{s}$ denote the derivatives corresponding to the thickness functions F_τ, F_s with respect to z. Considering the powers of z the derivatives $\partial F_\tau/\partial z, \partial F_s/\partial z = 0$, 1, $2z$, $3z^2$, $4z^3$, ..., $N_c z^{N_c-1}$. The subscripts ϱ, ζ represent the exponent of the quantities H_α, H_β, whereas ξ, η are the indices of the material constants $\bar{E}_{\xi\eta}^{(k)} = \bar{Q}_{\xi\eta}^{(k)}$ or $\bar{E}_{\xi\eta}^{(k)} = \bar{C}_{\xi\eta}^{(k)}$ for the kth ply [13]. The shear function $\kappa(z)$ allows to consider the shear correction needed in the theories in which the non-parabolic distribution of the shear stresses are assumed, such as in the first-order shear deformation theory $\kappa(z) = 5/6$. The governing equations of motion, within their boundary conditions, can be obtained through the Hamilton's Principle. In the present generalized approach each order τ has a set of three motion equations. As a function of the internal actions they assume the following compact matrix aspect

$$\mathbf{D}_\Omega^\star \mathbf{S}^{(\tau)} = \sum_{s=0}^{N_c+1} \mathbf{M}^{(\tau s)} \ddot{\mathbf{u}}^{(s)} \quad \text{for} \quad \tau = 0,1,2,\ldots,N_c,N_c+1 \tag{28}$$

where $\mathbf{D}_\Omega^\star$ is the equilibrium operator and $\mathbf{M}^{(\tau s)}$ is the inertia matrix. They can be found in explicit form in [20]. In detail, the mass matrix $\mathbf{M}_{(ij)}^{(\tau s)} = \delta_{ij} I_0^{(\tau s)}$ contains the inertia mass terms $I_0^{(\tau s)}$ for $i,j = 1,2,3$ and it can be evaluated as

$$I_0^{(\tau s)} = \sum_{k=1}^{N_L} \int_{z_k}^{z_{k+1}} \rho^{(k)} F_\tau F_s H_\alpha H_\beta dz \quad \text{for} \quad \tau,s = 0,1,2,\ldots,N_c,N_c+1 \tag{29}$$

where $\rho^{(k)}$ represents the mass density of the material per unit of volume of the kth ply. Combining the kinematic (21), constitutive (24) and the motion (28) equations, the fundamental system in terms of displacement parameters can be found

$$\sum_{s=0}^{N_c+1} \mathbf{L}^{(\tau s)} \mathbf{u}^{(s)} = \sum_{s=0}^{N_c+1} \mathbf{M}^{(\tau s)} \ddot{\mathbf{u}}^{(s)} \quad \text{for} \quad \tau = 0,1,2,\ldots,N_c,N_c+1 \tag{30}$$

where $\mathbf{L}^{(\tau s)} = \mathbf{D}_\Omega^\star \mathbf{A}^{(\tau s)} \mathbf{D}_\Omega$ [20] is the fundamental operator.

Boundary conditions must be introduced to solve the differential problem (30). Combining conveniently the kinematic and static conditions any boundary condition can be enforced. Generally, three configurations are the most classic ones [20], which are: clamped edge boundary conditions (C), free edge boundary conditions (F) and simply-supported edge boundary conditions (S). Only simply-supported structures are investigated in this paper in order to make the comparisons with the three-dimensional exact results:

$$\begin{aligned} &N_\alpha^{(\tau)} = 0,\ u_\beta^{(\tau)} = u_z^{(\tau)} = 0 \quad \tau = 0,1,2,\ldots,N_c,N_c+1 \quad \text{at} \quad \alpha = \alpha^0 \quad \text{or} \quad \alpha = \alpha^1 \quad \beta^0 \le \beta \le \beta^1 \\ &u_\alpha^{(\tau)} = 0,\ N_\beta^{(\tau)} = 0,\ u_z^{(\tau)} = 0 \quad \tau = 0,1,2,\ldots,N_c,N_c+1 \quad \text{at} \quad \beta = \beta^0 \quad \text{or} \quad \beta = \beta^1 \quad \alpha^0 \le \alpha \le \alpha^1 \end{aligned} \tag{31}$$

In this work higher-order layer-wise models are also taken into account (GDQ-LW) [77]. The theoretical developments follow an approach analogous to the previously reported scheme. The displacement field takes the form [14]

$$\mathbf{U}^{(k)} = \sum_{\tau=0}^{N_c+1} \mathbf{F}_{\tau}^{(k)} \mathbf{u}^{(k\tau)} \quad \text{for} \quad k = 1, 2, \ldots, N_L \tag{32}$$

Comparing (32) to (18) it is noted that each quantity is referred to each single layer (k). The thickness functions are assumed in the classic manner [14] as

$$F_{\tau}^{(k)} = \begin{cases} \dfrac{Q_0 - Q_1}{2} = \dfrac{1 - \bar{z}_k}{2} & \text{for} \quad \tau = 0 \\ Q_{\tau+1} - Q_{\tau-1} & \text{for} \quad \tau = 1, 2, \ldots, N_c \\ \dfrac{Q_0 + Q_1}{2} = \dfrac{1 + \bar{z}_k}{2} & \text{for} \quad \tau = N_c + 1 \end{cases} \tag{33}$$

where Q_τ are the Legendre polynomials recursively defined in [14] and $\bar{z}_k$ is the dimensionless thickness co-ordinate $\bar{z}_k(z) = z_k(z^{(k)}) \in [-1, 1]$. Considering the kth layer, it becomes $z_k = 2z^{(k)}/h_k$. The generalized displacements $u_\alpha^{(k0)}$, $u_\beta^{(k0)}$, $u_z^{(k0)}$ for $\tau = 0$ are the displacements at the bottom of the kth layer ($z^{(k)} = -h_k/2$), whereas $u_\alpha^{(k(N_c+1))}$, $u_\beta^{(k(N_c+1))}$, $u_z^{(k(N_c+1))}$ for $\tau = N_c+1$ are the displacements at the top of the kth layer ($z^{(k)} = +h_k/2$).

The strain-displacement relations for a 3D solid shell can be deducted from (19) adding the reference for the kth layer

$$\boldsymbol{\varepsilon}^{(k)} = \mathbf{D}^{(k)} \mathbf{U}^{(k)} = \mathbf{D}_Z^{(k)} \mathbf{D}_\Omega^{(k)} \mathbf{U}^{(k)} \quad \text{for} \quad k = 1, 2, \ldots, N_L \tag{34}$$

where $\mathbf{D}_Z^{(k)}$, $\mathbf{D}_\Omega^{(k)}$ have been explicitly reported in [14]. The strain component vector for the present higher-order layer-wise theory is evaluated substituting the displacement field (32) into the previous relation (34) as

$$\boldsymbol{\varepsilon}^{(k)} = \sum_{\tau=0}^{N_c+1} \mathbf{D}_Z^{(k)} \mathbf{D}_\Omega^{(k)} \mathbf{F}_\tau^{(k)} \mathbf{u}^{(k\tau)} = \sum_{\tau=0}^{N_c+1} \mathbf{Z}^{(k\tau)} \mathbf{D}_\Omega^{(k)} \mathbf{u}^{(k\tau)} = \sum_{\tau=0}^{N_c+1} \mathbf{Z}^{(k\tau)} \boldsymbol{\varepsilon}^{(k\tau)} \quad \text{for} \quad k = 1, 2, \ldots, N_L \tag{35}$$

where $\boldsymbol{\varepsilon}^{(k\tau)}$ is the τth order generalized strain component vector and the matrix $\mathbf{Z}^{(k\tau)}$ has been reported in extended form in [14]. Due to the present displacement field (32) the kinematic equations can be found

$$\boldsymbol{\varepsilon}^{(k\tau)} = \mathbf{D}_\Omega^{(k)} \mathbf{u}^{(k\tau)} \quad \text{for} \quad \tau = 0, 1, 2, \ldots, N_c, N_c + 1, \quad k = 1, 2, \ldots, N_L \tag{36}$$

A linear and elastic material constitutes the doubly-curved shell, thus the relationships between the stresses and strains for the kth ply are analogous to (22), as also reported extensively in [14], and the internal actions take the form

$$\mathbf{S}^{(k\tau)} = \sum_{s=0}^{N_c+1} \mathbf{A}^{(k\tau s)} \boldsymbol{\varepsilon}^{(ks)} \quad \text{for} \quad \tau = 0, 1, 2, \ldots, N_c, N_c + 1, \quad k = 1, 2, \ldots, N_L \tag{37}$$

where

$$\mathbf{A}^{(k\tau s)} = \sum_{k=1}^{N_L} \int_{-h_k/2}^{+h_k/2} \left(\mathbf{Z}^{(k\tau)} \right)^T \bar{\mathbf{C}}^{(k)} \mathbf{Z}^{(ks)} H_\alpha^{(k)} H_\beta^{(k)} dz^{(k)} \tag{38}$$

The τth order generalized internal action is indicated as $\mathbf{S}^{(k\tau)}$ and the elastic coefficients are $\mathbf{A}^{(k\tau s)}$ which are computed using the following formula [14]

$$
\begin{aligned}
A^{(k\tau s)}_{\xi\eta(\varrho\zeta)} &= \int_{-h_k/2}^{+h_k/2} \bar{C}^{(k)}_{\xi\eta} F^{(k)}_s F^{(k)}_\tau \frac{H^{(k)}_\alpha H^{(k)}_\beta}{\left(H^{(k)}_\alpha\right)^\varrho \left(H^{(k)}_\beta\right)^\zeta} dz^{(k)} \\
A^{(k\tilde{\tau}s)}_{\xi\eta(\varrho\zeta)} &= \int_{-h_k/2}^{+h_k/2} \bar{C}^{(k)}_{\xi\eta} F^{(k)}_s \frac{\partial F^{(k)}_\tau}{\partial z} \frac{H^{(k)}_\alpha H^{(k)}_\beta}{\left(H^{(k)}_\alpha\right)^\varrho \left(H^{(k)}_\beta\right)^\zeta} dz^{(k)} \qquad \text{for} \quad \tau, s = 0, 1, 2, \ldots, N_c, N_c+1 \\
A^{(k\tau\tilde{s})}_{\xi\eta(\varrho\zeta)} &= \int_{-h_k/2}^{+h_k/2} \bar{C}^{(k)}_{\xi\eta} \frac{\partial F^{(k)}_s}{\partial z} F^{(k)}_\tau \frac{H^{(k)}_\alpha H^{(k)}_\beta}{\left(H^{(k)}_\alpha\right)^\varrho \left(H^{(k)}_\beta\right)^\zeta} dz^{(k)} \qquad \text{for} \quad \xi, \eta = 1, 2, 3, 4, 5, 6 \\
A^{(k\tilde{\tau}\tilde{s})}_{\xi\eta(\varrho\zeta)} &= \int_{-h_k/2}^{+h_k/2} \bar{C}^{(k)}_{\xi\eta} \frac{\partial F^{(k)}_s}{\partial z} \frac{\partial F^{(k)}_\tau}{\partial z} \frac{H^{(k)}_\alpha H^{(k)}_\beta}{\left(H^{(k)}_\alpha\right)^\varrho \left(H^{(k)}_\beta\right)^\zeta} dz^{(k)} \qquad \text{for} \quad \varrho, \zeta = 0, 1, 2 \\
& \qquad\qquad\qquad\qquad\qquad\qquad\qquad\qquad\qquad\qquad\qquad\qquad\qquad\qquad\qquad\qquad \text{for} \quad k = 1, 2, \ldots, N_L
\end{aligned}
\tag{39}
$$

where τ and s indicate the thickness functions $F^{(k)}_\tau$ and $F^{(k)}_s$, respectively. A similar meaning is given to $\tilde{\tau}$, $\tilde{s}$ as far as the derivatives with respect to $z^{(k)}$ of the thickness functions are concerned. The subscripts ϱ, ζ are the exponents of the quantities $H^{(k)}_\alpha$, $H^{(k)}_\beta$ and ξ, η are the indices of the material constants for the generic kth lamina.

Using the Hamilton's Principle the equations of motion can be carried out. For the present layer-wise shell model a set of three equilibrium equations for each order τ can be found

$$
\mathbf{D}^{\star(k)}_\Omega \mathbf{S}^{(k\tau)} = \sum_{s=0}^{N_c+1} \mathbf{M}^{(k\tau s)} \ddot{\mathbf{u}}^{(ks)} \quad \text{for} \quad \tau = 0, 1, 2, \ldots, N_c, N_c+1, \quad k = 1, 2, \ldots, N_L \tag{40}
$$

where the equilibrium operator $\mathbf{D}^{\star(k)}_\Omega \mathbf{S}^{(k\tau)}$ and the inertia matrix $\mathbf{M}^{(k\tau s)}$ have been explicitly shown in [14]. The inertia terms take place into the inertia matrix as $\mathbf{M}^{(k\tau s)} = \delta_{ij} I^{(k\tau s)}_0$ for $i, j = 1, 2, 3$ and they are defined by the following expression

$$
I^{(k\tau s)}_0 = \int_{-h_k/2}^{+h_k/2} \rho^{(k)} F^{(k)}_\tau F^{(k)}_s H^{(k)}_\alpha H^{(k)}_\beta dz^{(k)} \quad \text{for} \quad \tau, s = 0, 1, 2, \ldots, N_c, N_c+1, \quad k = 1, 2, \ldots, N_L \tag{41}
$$

where $\rho^{(k)}$ is the mass density of the material per unit of volume of the kth lamina. Finally the fundamental equations in terms of generalized displacements take the form

$$
\sum_{s=0}^{N_c+1} \mathbf{L}^{(k\tau s)} \mathbf{u}^{(ks)} = \sum_{s=0}^{N_c+1} \mathbf{M}^{(k\tau s)} \ddot{\mathbf{u}}^{(ks)} \quad \text{for} \quad \tau = 0, 1, 2, \ldots, N_c, N_c+1, \quad k = 1, 2, \ldots, N_L \tag{42}
$$

where $\mathbf{L}^{(k\tau s)} = \mathbf{D}^{\star(k)}_\Omega \mathbf{A}^{(k\tau s)} \mathbf{D}^{(k)}_\Omega$ [14] is the fundamental operator. Since the approach is based on a layer-by-layer structure the compatibility conditions between the layers must be defined. In detail, the top displacements of the kth ply at each interface must be equal to the bottom displacements of the $(k+1)$th layer, as

$$
\begin{bmatrix} u^{(k\,\mathrm{top})}_\alpha \\ u^{(k\,\mathrm{top})}_\beta \\ u^{(k\,\mathrm{top})}_z \end{bmatrix} = \begin{bmatrix} u^{((k+1)\mathrm{bottom})}_\alpha \\ u^{((k+1)\mathrm{bottom})}_\beta \\ u^{((k+1)\mathrm{bottom})}_z \end{bmatrix} \rightarrow \begin{bmatrix} u^{(k(N_c+1))}_\alpha \\ u^{(k(N_c+1))}_\beta \\ u^{(k(N_c+1))}_z \end{bmatrix} = \begin{bmatrix} u^{((k+1)0)}_\alpha \\ u^{((k+1)0)}_\beta \\ u^{((k+1)0)}_z \end{bmatrix} \quad \text{for} \quad \begin{matrix} \tau = 0, 1, 2, \ldots, N_c, N_c+1 \\ k = 1, 2, \ldots, N_L - 1 \end{matrix} \tag{43}
$$

In conclusion, three types of boundary conditions can be reported, by means of the GDQ method, which have to be enforced for solving the partial differential system of equations [14]: clamped edge boundary conditions (C), free edge boundary conditions (F) and simply-supported edge boundary conditions (S). Only simply-supported structures are investigated in this paper in order to make the comparisons with the three-dimensional exact results:

$$\begin{array}{lllll} N_\alpha^{(k\tau)} = 0,\ u_\beta^{(k\tau)} = u_z^{(k\tau)} = 0 & \text{for} & \tau = 0,1,2,\ldots,N_c,N_c+1 & \text{at} & \alpha = \alpha^0 \quad \text{or} \quad \alpha = \alpha^1 \\ & & k = 1,2,\ldots,N_L & & \beta^0 \leq \beta \leq \beta^1 \\ u_\alpha^{(k\tau)} = 0,\ N_\beta^{(k\tau)} = 0,\ u_z^{(k\tau)} = 0 & \text{for} & \tau = 0,1,2,\ldots,N_c,N_c+1 & \text{at} & \beta = \beta^0 \quad \text{or} \quad \beta = \beta^1 \\ & & k = 1,2,\ldots,N_L & & \alpha^0 \leq \alpha \leq \alpha^1 \end{array} \tag{44}$$

4.1 Validation of the refined 2D shell models

In the previous section the theoretical background of equivalent single layer and layer-wise general higher-order 2D models have been presented. In order to solve the two differential systems, the GDQ method have been exploited. Considering a 1D problem on a domain described along the x axis, the GDQ method discretizes a general order derivative n as a weighted linear sum of the functional values at some pre-located discrete points as

$$\left.\frac{\partial^n f(x)}{\partial x^n}\right|_{x=x_m} = \sum_{k=1}^{I_N} \varsigma_{mk}^{(n)} f(x_k), \quad k = 1,2,\ldots,I_N \tag{45}$$

where I_N is the number of grid points chosen along the x axis and the weighting coefficients $\varsigma_{mk}^{(n)}$ are entirely defined by the well-known formulae provided by Shu [30]. On the other hand it is possible to use the same technique to numerically evaluate integrals, as suggested in [13]. The value of the integral of a generic function within the interval $[x_i, x_j]$ can be written in the form

$$\int_{x_i}^{x_j} f(x)dx = \sum_{k=1}^{I_N} \left(\varsigma_{jk}^{I} - \varsigma_{ik}^{I}\right) f(x_k), \quad k = 1,2,\ldots,I_N \tag{46}$$

where the coefficients ς_{jk}^{I}, ς_{ik}^{I}, have been explicitly defined in the book [13]. Integral expressions appear in the definition of the constitutive relations for the computation of engineering stiffnesses $A_{\xi\eta(\varrho\zeta)}^{(\tau s)}$, $A_{\xi\eta(\varrho\zeta)}^{(\tilde{\tau} s)}$, $A_{\xi\eta(\varrho\zeta)}^{(\tau \tilde{s})}$, $A_{\xi\eta(\varrho\zeta)}^{(\tilde{\tau}\tilde{s})}$ for the equivalent single layer theories and $A_{\xi\eta(\varrho\zeta)}^{(k\tau s)}$, $A_{\xi\eta(\varrho\zeta)}^{(k\tilde{\tau} s)}$, $A_{\xi\eta(\varrho\zeta)}^{(k\tau \tilde{s})}$, $A_{\xi\eta(\varrho\zeta)}^{(k\tilde{\tau}\tilde{s})}$ for the layer-wise ones.

The validation of the GDQ models is shown by Figure 4 where the same models used in section 3.1 are considered. For the present analyses a Chebyshev-Gauss-Lobatto grid [27] is taken into account

$$\begin{aligned} \alpha_i &= \left(1 - \cos\left(\frac{i-1}{I_N - 1}\pi\right)\right)\frac{\alpha^1 - \alpha^0}{2} + \alpha^0, \quad i = 1,2,\ldots,I_N, \quad \text{for} \quad \alpha \in \left[\alpha^0, \alpha^1\right] \\ \beta_j &= \left(1 - \cos\left(\frac{j-1}{I_M - 1}\pi\right)\right)\frac{\beta^1 - \beta^0}{2} + \beta^0, \quad j = 1,2,\ldots,I_M, \quad \text{for} \quad \beta \in \left[\beta^0, \beta^1\right] \end{aligned} \tag{47}$$

which demonstrated to be the one which leads to the most accurate solutions. The number of points for each direction α and β have been taken as $I_N = I_M$. Four different number of points $I_N = 11$, 15, 19, 25 are selected. It is noted that the convergence of the GDQ method is faster than the convergence given by the FE method. This feature is due to the higher order numerical scheme employed. The Reissner-Mindlin (RM) model has been considered for both GDQ and FE methods.

5 Results

This section proposes a detailed comparison between the 3D exact model discussed and validated in this paper (see Section 2) and several numerical models. Numerical models are the 2D and 3D FE models discussed and validated in Section 3, and the refined 2D GDQ models discussed and validated in Section 4.

5.1 Comparison between the two models

The first geometry considered in this investigation is a simply supported cylindrical shell (see part (a) of Figure 3). It has a radius of curvature $R_\alpha = 10$ m and an infinite radius of curvature R_β in β direction. The dimensions are $a = \frac{\pi}{3}R_\alpha$ and $b = 20$ m, and the thickness ratios are $R_\alpha/h = 1000$, 100, 10, 5. The second geometry is a simply supported spherical shell (see part (b) of Figure 3). It has radii of curvature $R_\alpha = R_\beta = 10$ m, dimensions $a = b = \frac{\pi}{3}R_\alpha$, and thickness ratios $R_\alpha/h = 1000$, 100, 10, 5. Both geometries will be considered as isotropic one-layered ($h_1 = h$), isotropic two-layered ($h_1 = h_2 = h/2$), isotropic three-layered ($h_1 = h_2 = h_3 = h/3$), three-layered composite cross-ply $90°/0°/90°$ ($h_1 = h_2 = h_3 = h/3$), four-layered composite cross-ply $90°/0°/90°/0°$ ($h_1 = h_2 = h_3 = h_4 = h/4$) and three layered sandwich (skins with $h_1 = h_3 = 0.2h$ and core with $h_2 = 0.6h$). The one-layered structures embed an aluminium alloy with Young modulus $E = 73$ GPa, Poisson ratio $\nu = 0.3$ and mass density $\rho = 2800$ kg/m^3. The two-layered structures have the bottom layer in aluminum alloy and the top layer in titanium alloy ($E = 114$ GPa, $\nu = 0.3$ and $\rho = 2768$ kg/m^3). The three-layered isotropic structures have the bottom layer in aluminum alloy, the mid layer in titanium alloy and the top layer in steel ($E = 210$ GPa, $\nu = 0.3$ and $\rho = 7850$ kg/m^3). The composite material for the three-layered and four-layered cross-ply structures has Young modulii $E_1 = 132.38$ GPa and $E_2 = E_3 = 10.756$ GPa, shear modulii $G_{12} = G_{13} = 5.6537$ GPa and $G_{23} = 3.603$ GPa, Poisson ratios $\nu_{12} = \nu_{13} = 0.24$ and $\nu_{23} = 0.49$, and mass density $\rho = 1600$ kg/m^3. Sandwich configurations have the skins in aluminium alloy (see one-layered, two-layered and three-layered isotropic structures) and the core is in PVC ($E = 0.18$ GPa, $\nu = 0.37$ and $\rho = 50$ kg/m^3).

For all the benchmarks, the first ten frequencies are calculated via the numerical models. From the visualization of these ten vibration modes, it is possible to understand the half-wave numbers m and n in the α and β directions. These half-wave numbers were used to calculate the same ten frequencies via the 3D exact model. Some frequencies could have been missed by the numerical codes, but they have not been added via the 3D exact model because this type of investigation is not the main aim of the paper. The main aim of the paper is to understand the differences between the numerical models (3D, refined 2D and classical 2D) and the 3D exact model in the analysis of the first ten frequencies given by the numerical codes. It is also important to understand which features influence these differences (geometry of the structures, materials, lamination sequences, thickness ratios, order of frequencies, vibration modes). The 3D exact solution gives infinite frequencies (I, II, III until to inf) for each couple of half-wave numbers (m,n).

The first benchmark considers a one-layered isotropic cylindrical shell (see Table 3 and Figure 5). Table 3 shows the first ten 3D frequencies for each thickness ratio R_α/h obtained for a given couple of half-wave numbers m and n. In the case of thin shells the first mode I is always considered for each frequency, for thick shells some frequencies are obtained by means of the second mode II. In the case of thick shells, in the first ten frequencies there were some modes with $w = 0$ that means in-plane modes. 2D FE results gave a good approximation for thin shells (R_α/h equals 1000 or 100) but they were unable to provide a good approximation for thick shells (R_α/h equals 10 or 5). 3D FE results worked well for thick shells. The GDQ results are given in the last three columns, GDQ-RM is based on the Reissner Mindlin model and GDQ-ESL and GDQ-LW are refined two-dimensional models with higher orders of expansion for the three displacement components based on the Equivalent Single Layer and Layer Wise approach, respectively. GDQ-RM results were similar to the 2D FE results because both

are 2D numerical models based on the Reissner-Mindlin theory. The GDQ-ESL and GDQ-LW models were always similar to the 3D exact results for each thickness ratio R_α/h and for each considered mode. Figure 5 shows the first five frequencies for the isotropic one-layered cylindrical shell with thickness ratio R_α/h=100. In the case of thin shells, in the first five frequencies there were not any in-plane vibration modes as demonstrated by the modes plotted via the GDQ method (see the left column) and the vibration modes plotted via the 3D exact solution (see the right column). In the 3D exact analysis, the vibration mode in the plane directions is known by means of the half-wave numbers m and n and only the three displacement components through the thickness direction are shown.

Tables 4-8 show similar results for cylindrical shells with more complicated laminations (two-layered and three layered isotropic cylindrical shells in Tables 4 and 5, three-layered and four-layered composite cylindrical shells with a lamination sequence $(90°/0°)$ in Tables 6 and 7, and sandwich cylindrical shells with foam core and isotropic skins in Table 7). Therefore, the main conclusions already drawn for the benchmark of Table 3 are confirmed. In this case the transverse anisotropy due to the inclusion of several layers with different elastic properties increases the differences between the results obtained with the 3D solution and refined 2D GDQ models and the results obtained with the Reissner-Mindilin theory (both FEM and GDQ models). In this case the GDQ equivalent single layer model uses the Murakami zigzag function in order to recover the zigzag form of displacements in the case of multilayered structures (GDQ-ZZ). When the GDQ-LW theory gives small errors with respect to GDQ-RM or GDQ-ZZ theories, this feature is due to the complication of imposing the simply supported boundary conditions for curved structures in the case of numerical models such as FE and GDQ models. These complications are not present in the case of Equivalent Single Layer models.

Tables 9-14 propose the same laminations already seen for the cylindrical shell for the case of a spherical shell. The conclusions and comments already seen for the cylindrical shells are confirmed for the spherical shells. In general, a complicated geometry of spherical shells (two radii of curvature in the α and β directions) gives bigger differences between the results obtained with the 3D models and refined 2D GDQ models and those obtained with the 2D Reissner-Mindilin theory (both FEM and GDQ models). Figure 6 shows the first five frequencies for the isotropic three-layered spherical shell with thickness ratio R_α/h=10. In the case of the thick shell, in the first five frequencies there were two in-plane modes (the fourth and fifth mode). These modes are clearly indicated by the GDQ images in the left hand column and by the three displacement components (plotted through the thickness direction) via the 3D exact solution in the right hand column. In these last two cases, it is clear how the transverse displacement w is zero for each value of the thickness coordinate z. Modes plotted in Figures 5 and 6 via the 3D exact solution are given as $u^* = U_k/|U_{MAX}|$, $v^* = V_k/|V_{MAX}|$, $w^* = W_k/|W_{MAX}|$ and $z^* = z/h$.

In the proposed numerical analyses, it has been observed that higher-order 2D models (in particular zigzag and layer-wise theories) and 3D analysis are mandatory for sandwich structures where the core has very different elastic properties with respect to the face sheets (higher values of transverse anisotropy).

Figures 7 and 8 show how the first (I) 3D modes changed with the half-wave numbers (m,n) in the case of simply supported two-layered isotropic cylindrical shells and three-layered composite spherical shells, respectively. In Figure 7, the n half-wave number was imposed equal 1, 2 and 3 and then the m value changed from 0 to 6. When the n values increased, the curves moved to higher values of frequency. The minimum in frequency was obtained for an m value different from zero. This value of m, which gives the minimum in frequency, moves to higher values when the n half-wave number increases. This feature is more evident for the case R_α/h=100. Similar considerations are confirmed for the spherical composite shell investigated in the Figure 8 for the thick (R_α/h=100) and thin (R_α/h=10) cases.

6 Conclusions

This paper has proposed an exact three-dimensional model and several refined and classical two-dimensional generalized differential quadrature (GDQ) methods for the free vibration analysis of one-layered and multilayered plates and shells. Comparisons with a commercial finite element (FE) code have been proposed (for the cases of cylindrical and spherical shells) in order to explain the method used for the comparison between exact 3D and numerical 2D models and to see the possible differences between an exact 3D solution and numerical 2D solutions.

The exact 3D solution gives infinite vibration modes (for all the possible combinations of half-wave numbers (m,n)). A 2D numerical code gives a finite number of vibration modes because it uses a finite number of degrees of freedom in the plane and in the thickness direction. A possible method to make a 3D versus 2D comparison is to calculate the frequencies via the 2D numerical code and then to evaluate the 3D exact frequencies by means of the appropriate half-wave numbers (obtained via a correct visualization of the vibration modes via the GDQ or FE method). It is obvious that the 3D analysis could give some frequencies that are missed by the 2D numerical codes, but this investigation is not the main aim of the paper. The paper tries to explain what could be the advantages and the limitations of 2D numerical codes. A typical 2D FE code uses a Reissner-Mindlin model for the approximation of displacement components through the thickness direction. Results in this paper show how this model employed by commercial FE codes could give errors for thick and moderately thick structures, complicated lamination sequences, higher order frequencies and particular vibration modes. In these cases, the use of 3D finite elements or refined 2D GDQ models is mandatory.

The behavior of frequency values and vibration modes versus imposed half-wave numbers has been investigated via the 3D exact model. The behavior is simple and easily predictable for plate structures because the increasing of m and/or n values gives bigger frequency values. In the case of shell geometry there is a coupling between the displacement components due to the curvature. For this reason, when the half-wave number n is imposed, the minimum of frequency is obtained for a value of the half-wave number m different from 0. When the half-wave number n increases, the frequency versus m curves move to higher values of frequencies and the minimum in frequency moves to higher values of the half-wave number m. These last considerations are very similar for one-layered and multilayered structures.

References

[1] A.W. Leissa, *Vibration of Plates*, NASA SP-160, Washington, 1969.

[2] A.W. Leissa, *Vibration of Shells*, NASA SP-288, Washington, 1973.

[3] S. Werner, *Vibrations of Shells and Plates*, 3rd edition: revised and expanded, CRC Press, New York: Marcel Dekker Inc., 2004.

[4] S. Brischetto and E. Carrera, Importance of higher order modes and refined theories in free vibration analysis of composite plates, *Journal of Applied Mechanics*, 77, 1-14, 2010.

[5] S. Brischetto, Exact elasticity solution for natural frequencies of functionally graded simply-supported structures, *CMES: Computer Modeling in Engineering & Sciences*, 95, 391-430, 2013.

[6] S. Brischetto, Three-dimensional exact free vibration analysis of spherical, cylindrical, and flat one-layered panels, *Shock and Vibration*, 2014, 1-29, 2014.

[7] S. Brischetto, An exact 3D solution for free vibrations of multilayered cross-ply composite and sandwich plates and shells, *International Journal of Applied Mechanics*, 6, 1-42, 2014.

[8] S. Brischetto and R. Torre, Exact 3D solutions and finite element 2D models for free vibration analysis of plates and cylinders, *Curved and Layered Structures*, 1, 59-92, 2014.

[9] S. Brischetto, A continuum elastic three-dimensional model for natural frequencies of single-walled carbon nanotubes, *Composites Part B: Engineering*, 61, 222-228, 2014.

[10] S. Brischetto, A continuum shell model including van der Waals interaction for free vibrations of double-walled carbon nanotubes, *CMES: Computer Modeling in Engineering & Sciences*, 104, 305-327, 2015.

[11] Straus7, Straus7 Release 2.3.6 finite element analysis system. Sydney, Australia.

[12] F. Tornabene, *Meccanica delle Strutture a Guscio in Materiale Composito*, Società Editrice Esculapio, Bologna (Italy), 2012.

[13] F. Tornabene and N. Fantuzzi, *Mechanics of Laminated Composite Doubly-Curved Shell Structures. The Generalized Differential Quadrature Method and the Strong Formulation Finite Element Method*, Società Editrice Esculapio, Bologna (Italy), 2014.

[14] F. Tornabene, General higher order layer-wise theory for free vibrations of doubly-curved laminated composite shells and panels, *Mechanics of Advanced Materials and Structures*, In Press, 2015.

[15] F. Tornabene, N. Fantuzzi and M. Bacciocchi, Free vibrations of free-form doubly-curved shells made of functionally graded materials using higher-order equivalent single layer theories, *Composites Part B: Engineering*, 67, 490-509, 2014.

[16] F. Tornabene, N. Fantuzzi and M. Bacciocchi, The local GDQ method applied to general higher-order theories of doubly-curved laminated composite shells and panels: the free vibration analysis, *Composite Structures*, 116, 637-660, 2014.

[17] F. Tornabene, N. Fantuzzi, E. Viola and J.N. Reddy, Winkler-Pasternak foundation effect on the static and dynamic analyses of laminated doubly-curved and degenerate shells and panels, *Composites Part B: Engineering*, 57, 269-296, 2014.

[18] F. Tornabene, N. Fantuzzi, E. Viola and A.J.M. Ferreira, Radial basis function method applied to doubly-curved laminated composite shells and panels with a general higher-order equivalent single layer theory, *Composites Part B: Engineering*, 55, 642-659, 2013.

[19] F. Tornabene and A. Ceruti, Mixed static and dynamic optimizazion of four-parameter functionally graded completely doubly-curved and degenerate shells and panels using GDQ method, *Mathematical Problems in Engineering* Vol. 2013, Article ID 867079, 1-33, 2013.

[20] F. Tornabene, E. Viola and N. Fantuzzi, General higher-order equivalent single layer theory for free vibrations of doubly-curved laminated composite shells and panels, *Composite Structures*, 104, 94-117, 2013.

[21] F. Tornabene and A. Ceruti, Free-form laminated doubly-curved shells and panels of revolution on Winkler-Pasternak elastic foundations: a 2D GDQ solution for static and free vibration analysis, *World Journal of Mechanics* 3, 1-25, 2013.

[22] E. Viola, F. Tornabene and N. Fantuzzi, General higher-order shear deformation theories for the free vibration analysis of completely doubly-curved laminated shells and panels, *Composite Structures* 95, 639-666, 2013.

[23] A.J.M. Ferreira, E. Carrera, M. Cinefra, E. Viola, F. Tornabene, N. Fantuzzi and A.M. Zenkour, Analysis of thick isotropic and cross-ply laminated plates by generalized differential quadrature method and a unified formulation, *Composites Part B: Engineering* 58, 544-552, 2014.

[24] A.J.M. Ferreira, E. Viola, F. Tornabene, N. Fantuzzi and A.M. Zenkour, Analysis of sandwich plates by generalized differential quadrature method, *Mathematical Problems in Engineering* Vol. 2013, Article ID 964367, 1-12, 2013.

[25] F. Tornabene, A. Liverani and G. Caligiana, General anisotropic doubly-curved shell theory: a differential quadrature solution for free vibrations of shells and panels of revolution with a free-form meridian, *Journal of Sound & Vibration*, 331, 4848-4869, 2012.

[26] F. Tornabene, A. Liverani and G. Caligiana, FGM and laminated doubly-curved shells and panels of revolution with a free-form meridian: a 2-D GDQ solution for free vibrations, *International Journal of Mechanical Sciences*, 53, 446-470, 2011.

[27] F. Tornabene, Free vibrations of anisotropic doubly-curved shells and panels of revolution with a free-form meridian resting on Winkler-Pasternak elastic foundations, *Composite Structures*, 94, 186-206, 2011.

[28] F. Tornabene, 2-D GDQ solution for free vibrations of anisotropic doubly-curved shells and panels of revolution, *Composite Structures*, 93, 1854-1876, 2011.

[29] F. Tornabene, Free vibrations of laminated composite doubly-curved shells and panels of revolution via the GDQ method, *Computer Methods in Applied Mechanics and Engineering*, 200, 931-952, 2011.

[30] C. Shu and B.E. Richard, Parallel simulation of incompressible viscous flows by generalized differential quadrature, *Computing Systems in Engineering*, 3, 271-281, 1992.

[31] C.W. Bert and M. Malik, Differential quadrature method in computational mechanics: a review, *Applied Mechanics Reviews*, 49, 1-28.

[32] F. Tornabene, N. Fantuzzi, F. Ubertini and E. Viola, Strong formulation finite element method based on differential quadrature: a survey, *Applied Mechanics Reviews* 67, 020801-1-55, 2015.

[33] F. Tornabene, N. Fantuzzi and M. Bacciocchi, The strong formulation finite element method: stability and accuracy, *Fracture and Structural Integrity*, 29, 251-265, 2014.

[34] N. Fantuzzi, F. Tornabene and E. Viola, Four-parameter functionally graded cracked plates of arbitrary shape: a GDQFEM solution for free vibrations, *Mechanics of Advanced Materials and Structures*, in Press, 2015.

[35] N. Fantuzzi, M. Bacciocchi, F. Tornabene, E. Viola and A.J.M. Ferreira, Radial basis functions based on differential quadrature method for the free vibration of laminated composite arbitrary shaped plates, *Composites Part B: Engineering*, In press, 2015.

[36] E. Viola, M. Miniaci, N. Fantuzzi and A. Marzani, Vibration analysis of multi-stepped and multi-damaged parabolic arches using GDQ, *Curved and Layered Structures*, 2, 28-49, 2015.

[37] N. Fantuzzi, F. Tornabene, E. Viola and A.J.M. Ferreira, A strong formulation finite element method (SFEM) based on RBF and GDQ techniques for the static and dynamic analyses of laminated plates of arbitrary shape, *Meccanica*, 49, 2503-2542, 2014.

[38] N. Fantuzzi, New insights into the strong formulation finite element method for solving elastostatic and elastodynamic problems, *Curved and Layered Structures* 1, 93-126, 2014.

[39] N. Fantuzzi, F. Tornabene and E. Viola, Generalized differential quadrature finite element method for vibration analysis of arbitrarily shaped membranes, *International Journal of Mechanical Sciences*, 79, 216-251, 2014.

[40] E. Viola, F. Tornabene and N. Fantuzzi, Generalized differential quadrature finite element method for cracked composite structures of arbitrary shape, *Composite Structures*, 106, 815-834, 2013.

[41] W.-Q. Chen, H.-J. Ding and R.-Q. Xu, On exact analysis of free vibrations of embedded transversely isotropic cylindrical shells, *International Journal of Pressure Vessels and Piping*, 75, 961-966, 1998.

[42] B. Gasemzadeh, R. Azarafza, Y. Sahebi and A. Motallebi, Analysis of free vibration of cylindrical shells on the basis of three dimensional exact elasticity theory, *Indian Journal of Science and Technology*, 5, 3260-3262, 2012.

[43] N.N. Huang, Exact analysis for three-dimensional free vibrations of cross-ply cylindrical and doubly-curved laminates, *Acta Mechanica*, 108, 23-34, 1995.

[44] J.N. Sharma, D.K. Sharma and S.S. Dhaliwal, Three-dimensional free vibration analysis of a viscothermoelastic hollow sphere, *Open Journal of Acoustics*, 2, 12-24, 2012.

[45] J.N. Sharma and N. Sharma, Three-dimensional free vibration analysis of a homogeneous transradially isotropic thermoelastic sphere, *Journal of Applied Mechanics*, 77, 1-9, 2010.

[46] K.P. Soldatos and J. Ye, Axisymmetric static and dynamic analysis of laminated hollow cylinders composed of monoclinic elastic layers, *Journal of Sound and Vibration*, 184, 245-259, 1995.

[47] A.E. Armenakas, D.C. Gazis and G. Herrmann, *Free Vibrations of Circular Cylindrical Shells*, Pergamon Press, Oxford, 1969.

[48] A. Bhimaraddi, A higher order theory for free vibration analysis of circular cylindrical shells, *International Journal of Solids and Structures*, 20, 623-630, 1984.

[49] H. Zhou, W. Li, B. Lv and W.L. Li, Free vibrations of cylindrical shells with elastic-support boundary conditions, *Applied Acoustics*, 73, 751-756, 2012.

[50] S.M.R. Khalili, A. Davar and K.M. Fard, Free vibration analysis of homogeneous isotropic circular cylindrical shells based on a new three-dimensional refined higher-order theory, *International Journal of Mechanical Sciences*, 56, 1-25, 2012.

[51] S.S. Vel, Exact elasticity solution for the vibration of functionally graded anisotropic cylindrical shells, *Composite Structures*, 92, 2712-2727, 2010.

[52] C.T. Loy and K.Y. Lam, Vibration of thick cylindrical shells on the basis of three-dimensional theory of elasticity, *Journal of Sound and Vibration*, 226, 719-737, 1999.

[53] Y. Wang, R. Xu, H. Ding and J. Chen, Three-dimensional exact solutions for free vibrations of simply supported magneto-electro-elastic cylindrical panels, *International Journal of Engineering Science*, 48, 1778-1796, 2010.

[54] E. Efraim and M. Eisenberger, Exact vibration frequencies of segmented axisymmetric shells, *Thin-Walled Structures*, 44, 281-289, 2006.

[55] J.-H. Kanga and A.W. Leissa, Three-dimensional vibrations of thick spherical shell segments with variable thickness, *International Journal of Solids and Structures*, 37, 4811-4823, 2000.

[56] K.M. Liew, L.X. Peng and T.Y. Ng, Three-dimensional vibration analysis of spherical shell panels subjected to different boundary conditions, *International Journal of Mechanical Sciences*, 44, 2103-2117, 2002.

[57] C. Shu, An efficient approach for free vibration analysis of conical shells, *International Journal of Mechanical Sciences*, 38, 935-949, 1996.

[58] C. Shu, Free vibration analysis of composite laminated conical shells by generalized differential quadrature, *Journal of Sound & Vibration*, 194, 587-604, 1996.

[59] E. Viola and F. Tornabene, Vibration analysis of conical shell structures using GDQ method, *Far East Journal of Applied Mathematics* 25, 23-39, 2006.

[60] F. Tornabene, E. Viola and D.J. Inman, 2-D differential quadrature solution for vibration analysis of functionally graded conical, cylindrical shell and annular plate structures, *Journal of Sound & Vibration*, 328, 259-290, 2009.

[61] F. Tornabene, Free vibration analysis of functionally graded conical, cylindrical shell and annular plate structures with a four-parameter power-law distribution, *Computer Methods in Applied Mechanics and Engineering*, 198, 2911-2935, 2009.

[62] F. Tornabene and E. Viola, Free vibrations of four-parameter functionally graded parabolic panels and shells of revolution, *European Journal of Mechanics - A/Solids*, 28, 991-1013, 2009.

[63] E. Viola and F. Tornabene, Free vibrations of three parameter functionally graded parabolic panels of revolution, *Mechanics Research Communications*, 36, 587-594, 2009.

[64] F. Tornabene and E. Viola, Free vibration analysis of functionally graded panels and shells of revolution, *Meccanica* 44, 255-281, 2009.

[65] F. Tornabene and E. Viola, 2-D solution for free vibrations of parabolic shells using generalized differential quadrature method, *European Journal of Mechanics - A/Solids*, 27, 1001-1025, 2008.

[66] F. Tornabene and E. Viola, Vibration analysis of spherical structural elements using the GDQ method, *Computers & Mathematics with Applications*, 53, 1538-1560, 2007.

[67] A. Messina, Three dimensional free vibration analysis of cross-ply laminated plates through 2D and exact models, *3rd International Conference on Integrity, Reliability and Failure*, Porto (Portugal), 20-24 July 2009.

[68] F.B. Hildebrand, E. Reissner and G.B. Thomas, *Notes on the Foundations of the Theory of Small Displacements of Orthotropic Shells*, NACA Technical Note No. 1833, Washington, 1949.

[69] G.B. Gustafson, *Systems of Differential Equations*, free available on http://www.math.utah.edu/gustafso/, accessed on 16th September 2014.

[70] W.E. Boyce and R.C. DiPrima, *Elementary Differential Equations and Boundary Value Problems*, John Wiley & Sons, Ltd., New York, 2001.

[71] D. Zwillinger, *Handbook of Differential Equations*, Academic Press, New York, 1997.

[72] C. Molery and C. Van Loan, Nineteen dubious ways to compute the exponential of a matrix, twenty-five years later, *SIAM Review*, 45, 1-46, 2003.

[73] G. Giunta, F. Biscani, S. Belouettar and E. Carrera, Hierarchical modelling of doubly curved laminated composite shells under distributed and localised loadings, *Composites Part B: Engineering*, 42, 682-691, 2011.

[74] E. Carrera and G. Giunta, Exact, hierarchical solutions for localized loadings in isotropic, laminated, and sandwich shells, *Journal of Pressure Vessel Technology, Transactions of the ASME*, 131, 041202, 2009.

[75] G. Giunta, F. Biscani, S. Belouettar, A.J.M. Ferreira and E. Carrera , Free vibration analysis of composite beams via refined theories, *Composites Part B: Engineering*, 44, 540-552, 2013.

[76] G. Giunta, N. Metla, Y. Koutsawa and S. Belouettar, Free vibration and stability analysis of three-dimensional sandwich beams via hierarchical models, *Composites Part B: Engineering*, 47, 326-338, 2013.

[77] E. Carrera, S. Brischetto and P. Nali, *Plates and Shells for Smart Structures: Classical and Advanced Theories for Modeling and Analysis*, John Wiley & Sons, Ltd., New Delhi, 2011.

[78] E. Carrera and S. Brischetto, Analysis of thickness locking in classical, refined and mixed multilayered plate theories, *Composite Structures*, 82, 549-562, 2008.

[79] E. Carrera and S. Brischetto, Analysis of thickness locking in classical, refined and mixed theories for layered shells, *Composite Structures*, 85, 83-90, 2008.

		$N_L = 2$		$N_L = 4$		$N_L = 10$	
m,n	mode	3D [43]	Present 3D	3D [43]	Present 3D	3D [43]	Present 3D
1,1	I	1.8971	1.8971	2.3415	2.3415	2.4930	2.4930
1,1	II	18.813	18.813	21.545	21.545	22.387	22.387
1,1	III	20.169	20.169	22.902	22.902	23.694	23.694
1,2	I	4.4492	4.4492	4.9620	4.9620	5.3017	5.3017
1,3	I	7.8195	7.8195	8.0752	8.0753	8.5254	8.5253
2,1	I	4.3485	4.3485	4.8493	4.8493	5.1853	5.1853
2,2	I	6.0384	6.0384	6.5486	6.5486	6.9739	6.9739
2,3	I	8.8895	8.8895	9.1438	9.1438	9.6347	9.6346
3,1	I	7.7503	7.7503	7.9573	7.9573	8.3952	8.3950
3,2	I	8.9012	8.9012	9.1290	9.1290	9.6122	9.6120
3,3	I	11.103	11.103	11.164	11.164	11.686	11.686

Table 1: First assessment for the 3D exact solution, simply supported composite cylindrical panel with thickness ratio $R_\alpha/h = 20$. Circular frequencies $\bar{\omega} = \omega R_\alpha \sqrt{\frac{\rho}{E_0}}$ for several physical layers N_L, lamination sequence $(0°/90°/0°/90°/\ldots)$ and half-wave numbers m and n.

		$N_L = 2$		$N_L = 4$		$N_L = 10$	
m,n	mode	3D [43]	Present 3D	3D [43]	Present 3D	3D [43]	Present 3D
1,1	I	4.6238	4.6240	5.8070	5.8070	6.2293	6.2293
1,2	I	10.753	10.753	12.134	12.134	13.050	13.050
1,3	I	19.130	19.130	19.846	19.845	21.042	21.042
2,1	I	10.864	10.864	12.188	12.188	13.076	13.076
2,2	I	14.909	14.909	16.298	16.298	17.432	17.432
2,3	I	21.961	21.961	22.719	22.719	24.027	24.027
3,1	I	19.315	19.315	19.932	19.931	21.082	21.081
3,2	I	22.053	22.053	22.757	22.757	24.045	24.045
3,3	I	27.483	27.483	27.790	27.790	29.189	29.189

Table 2: Second assessment for the 3D exact solution, simply supported composite spherical panel with thickness ratio $R_\alpha/h = 50$. Circular frequencies $\bar{\omega} = \omega R_\alpha \sqrt{\frac{\rho}{E_0}}$ for several physical layers N_L, lamination sequence $(0°/90°/0°/90°/\ldots)$ and half-wave numbers m and n.

m,n	Mode	3D exact	3D FE	2D FE	GDQ-RM	GDQ-ESL	GDQ-LW
$R_\alpha/h = 1000$							
3,1	I	3.123	3.126	3.131	3.123	3.123	3.123
4,1	I	3.816	3.824	3.825	3.816	3.816	3.816
2,1	I	5.216	5.216	5.223	5.216	5.215	5.215
5,1	I	5.625	5.640	5.642	5.625	5.625	5.625
4,2	I	6.402	6.406	6.416	6.402	6.402	6.402
5,2	I	6.672	6.685	6.692	6.672	6.672	6.672
6,1	I	8.014	8.039	8.047	8.014	8.014	8.014
6,2	I	8.516	8.540	8.551	8.516	8.516	8.516
3,2	I	9.037	9.037	9.050	9.037	9.037	9.037
5,3	I	9.460	9.469	9.487	9.460	9.460	9.460
$R_\alpha/h = 100$							
2,1	I	10.41	10.42	10.45	10.42	10.41	10.41
1,1	I	16.68	16.67	16.73	16.68	16.68	16.68
3,1	I	20.26	20.27	20.28	20.26	20.26	20.26
2,2	I	20.34	20.34	20.40	20.35	20.34	20.34
3,2	I	23.58	23.60	23.62	23.59	23.58	23.58
3,3	I	30.34	30.35	30.40	30.35	30.34	30.34
2,3	I	33.59	33.59	33.65	33.60	33.59	33.59
4,1	I	35.58	35.62	35.64	35.57	35.58	35.58
4,2	I	37.70	37.74	37.76	37.70	37.70	37.70
3,4	I	39.33	39.34	39.40	39.34	39.33	39.33
$R_\alpha/h = 10$							
1,1	I	28.72	28.72	28.69	28.80	28.72	28.72
1,2	I	57.69	57.69	57.70	57.79	57.69	57.69
0,1	I	79.16	79.16	79.24	79.16	79.16	79.16
2,1	I	85.46	85.47	85.04	85.28	85.46	85.46
1,3	I	89.46	89.46	89.54	89.51	89.46	89.46
2,2	I	102.2	102.2	101.7	102.0	102.2	102.2
1,4	I	125.6	125.6	125.7	125.5	125.6	125.6
2,3	I	130.1	130.1	129.4	129.8	130.1	130.1
1,0	II($w = 0$)	151.3	151.2	151.3	151.3	151.3	151.3
0,2	II($w = 0$)	158.3	158.3	158.5	158.3	158.3	158.3
$R_\alpha/h = 5$							
1,1	I	47.66	47.66	47.09	47.71	47.66	47.66
0,1	I	79.16	79.16	79.35	79.16	79.16	79.16
1,2	I	85.35	85.35	84.59	85.34	85.35	85.35
1,3	I	134.8	134.8	133.8	134.4	134.8	134.8
2,1	I	148.5	148.5	146.0	147.4	148.5	148.5
1,0	II($w = 0$)	151.4	151.4	151.3	151.4	151.4	151.4
0,2	II($w = 0$)	158.3	158.3	158.7	158.3	158.3	158.3
2,2	I	172.6	172.6	169.4	171.2	172.6	172.6
1,1	II	175.5	175.5	176.1	175.5	175.5	175.5
1,4	I	192.6	192.6	191.2	191.4	192.6	192.6

Table 3: First benchmark, simply supported cylindrical shell made of aluminium alloy with thickness ratios $R_\alpha/h = 1000$, $R_\alpha/h = 100$, $R_\alpha/h = 10$ and $R_\alpha/h = 5$. First ten frequencies in Hz, comparison between the present 3D exact solution and several numerical solutions.

m,n	Mode	3D exact	3D FE	2D FE	GDQ-RM	GDQ-ZZ	GDQ-LW
$R_\alpha/h = 1000$							
3,1	I	3.518	3.523	3.527	3.518	3.518	3.521
4,1	I	4.263	4.281	4.272	4.263	4.262	4.269
2,1	I	5.917	5.917	5.925	5.916	5.916	5.917
5,1	I	6.271	6.317	6.289	6.271	6.271	6.282
4,2	I	7.221	7.232	7.237	7.221	7.221	7.225
5,2	I	7.471	7.510	7.493	7.471	7.471	7.480
6,1	I	8.931	9.027	8.967	8.931	8.931	8.947
6,2	I	9.503	9.595	9.541	9.503	9.503	9.519
3,2	I	10.25	10.25	10.26	10.25	10.25	10.25
5,3	I	10.66	10.69	10.69	10.66	10.66	10.66
$R_\alpha/h = 100$							
2,1	I	11.65	11.65	11.69	11.66	11.65	11.65
1,1	I	18.92	18.92	18.98	18.93	18.92	18.92
3,1	I	22.56	22.58	22.58	22.56	22.56	22.56
2,2	I	22.97	22.97	23.02	22.97	22.97	22.96
3,2	I	26.33	26.34	26.37	26.33	26.33	26.33
3,3	I	34.00	34.02	34.06	34.01	34.00	34.00
2,3	I	38.00	38.01	38.07	38.01	38.00	38.00
4,1	I	39.61	39.67	39.67	39.61	39.61	39.62
4,2	I	41.99	42.04	42.05	41.99	41.99	42.00
3,4	I	44.18	44.20	44.26	44.19	44.18	44.18
$R_\alpha/h = 10$							
1,1	I	32.11	32.11	32.03	32.18	32.11	32.11
1,2	I	64.74	64.74	64.76	64.87	64.74	64.69
0,1	II($w = 0$)	90.60	90.60	90.64	90.60	90.60	90.35
2,1	I	94.60	94.61	93.93	94.40	94.61	94.74
1,3	I	100.1	100.1	100.3	100.2	100.1	100.1
2,2	I	113.3	113.3	112.5	113.2	113.3	113.5
1,4	I	140.3	140.3	140.5	140.3	140.3	140.3
2,3	I	144.4	144.4	143.6	144.3	144.4	144.6
1,0	II($w = 0$)	171.2	171.2	171.2	171.2	171.2	170.8
0,2	II($w = 0$)	181.2	181.2	181.3	181.2	181.2	180.7
$R_\alpha/h = 5$							
1,1	I	52.79	52.79	52.03	52.84	52.79	52.90
0,1	II($w = 0$)	91.32	91.32	91.43	91.33	91.33	90.83
1,2	I	95.04	95.04	94.21	95.14	95.04	95.10
1,3	I	150.0	150.0	149.1	149.9	150.0	150.2
2,1	I	163.6	163.6	160.5	162.8	163.6	164.2
1,0	II($w = 0$)	170.9	170.9	170.7	170.9	170.9	170.4
0,2	II($w = 0$)	182.5	182.5	182.7	182.6	182.5	181.5
2,2	I	190.6	190.6	186.8	189.7	190.6	191.1
1,1	II	198.8	198.8	199.2	198.8	198.8	198.0
1,4	I	214.4	214.4	212.9	213.7	214.4	214.6

Table 4: Second benchmark, simply supported cylindrical shell made of aluminium alloy and titanium alloy with thickness ratios $R_\alpha/h = 1000$, $R_\alpha/h = 100$, $R_\alpha/h = 10$ and $R_\alpha/h = 5$. First ten frequencies in Hz, comparison between the present 3D exact solution and several numerical solutions.

m,n	Mode	3D exact	3D FE	2D FE	GDQ-RM	GDQ-ZZ	GDQ-LW
			$R_\alpha/h = 1000$				
3,1	I	3.259	3.364	3.265	3.259	3.259	3.262
4,1	I	3.889	4.163	3.894	3.889	3.889	3.895
2,1	I	5.548	5.573	5.555	5.548	5.548	5.549
5,1	I	5.701	6.199	5.711	5.701	5.701	5.711
4,2	I	6.706	7.321	6.718	6.706	6.706	6.710
5,2	I	6.847	8.196	6.862	6.847	6.847	6.856
6,1	I	8.114	8.926	8.137	8.113	8.114	8.129
6,2	I	8.656	9.798	8.682	8.656	8.656	8.671
3,2	I	9.600	10.87	9.612	9.600	9.600	9.602
5,3	I	9.876	12.05	9.899	9.876	9.876	9.883
			$R_\alpha/h = 100$				
2,1	I	10.67	10.67	10.69	10.67	10.67	10.69
1,1	I	17.76	17.76	17.80	17.76	17.76	17.77
3,1	I	20.50	20.51	20.48	20.49	20.50	20.55
2,2	I	21.38	21.38	21.41	21.38	21.38	21.39
3,2	I	24.03	24.04	24.03	24.03	24.03	24.08
3,3	I	31.24	31.25	31.25	31.24	31.24	31.29
2,3	I	35.49	35.50	35.53	35.50	35.49	35.52
4,1	I	35.97	36.02	35.95	35.97	35.97	36.07
4,2	I	38.16	38.20	38.14	38.15	38.16	38.25
3,4	I	40.76	40.77	40.78	40.76	40.76	40.81
			$R_\alpha/h = 10$				
1,1	I	29.47	29.47	29.24	29.52	29.48	29.65
1,2	I	59.78	59.78	59.57	59.85	59.79	60.06
0,1	II($w = 0$)	84.20	84.20	84.17	84.20	84.20	84.24
2,1	I	85.60	85.60	85.77	85.58	85.69	86.44
1,3	I	92.05	92.05	91.83	92.12	92.09	92.56
2,2	I	102.7	102.7	101.1	102.8	102.8	103.6
1,4	I	128.3	128.3	127.9	128.5	128.4	129.2
2,3	I	131.1	131.1	129.2	131.3	131.3	132.2
1,0	II($w = 0$)	159.2	159.2	160.1	159.2	159.2	159.5
0,2	II($w = 0$)	168.4	168.4	166.0	168.4	168.4	168.5
			$R_\alpha/h = 5$				
1,1	I	47.84	47.84	46.82	47.90	47.89	48.59
0,1	II($w = 0$)	84.05	84.05	85.43	84.05	84.05	84.15
1,2	I	86.66	86.66	87.08	86.85	86.78	87.76
1,3	I	136.5	136.5	134.8	136.9	136.8	138.3
2,1	I	147.1	147.1	142.6	147.6	147.5	149.7
1,0	II($w = 0$)	157.4	157.5	158.7	157.5	157.4	158.2
0,2	II($w = 0$)	168.1	168.1	166.4	168.1	168.1	168.3
2,2	I	171.5	171.5	173.7	172.3	172.1	174.4
1,1	II	183.4	183.5	185.7	183.5	183.5	184.1
1,4	I	194.5	194.5	191.7	195.3	195.1	197.1

Table 5: Third benchmark, simply supported cylindrical shell made of aluminium alloy, titanium alloy and steel with thickness ratios $R_\alpha/h = 1000$, $R_\alpha/h = 100$, $R_\alpha/h = 10$ and $R_\alpha/h = 5$. First ten frequencies in Hz, comparison between the present 3D exact solution and several numerical solutions.

m,n	Mode	3D exact	3D FE	2D FE	GDQ-RM	GDQ-ZZ	GDQ-LW
$R_\alpha/h = 1000$							
4,1	I	2.752	2.785	2.755	2.752	2.752	2.752
3,1	I	3.209	3.234	3.213	3.210	3.210	3.210
5,1	I	3.435	3.484	3.441	3.435	3.435	3.435
6,1	I	4.700	4.782	4.714	4.701	4.700	4.700
5,2	I	5.232	5.274	5.244	5.232	5.232	5.232
6,2	I	5.602	5.649	5.620	5.603	5.602	5.602
2,1	I	5.634	5.683	5.637	5.634	5.634	5.634
4,2	I	6.075	6.096	6.084	6.075	6.075	6.075
7,1	I	6.316	6.459	6.344	6.317	6.316	6.316
7,2	I	6.794	6.938	6.824	6.796	6.794	6.794
$R_\alpha/h = 100$							
2,1	I	7.717	7.719	7.723	7.718	7.718	7.717
3,1	I	12.02	12.03	12.02	12.02	12.02	12.02
1,1	I	13.43	13.43	13.44	13.43	13.43	13.43
3,2	I	15.59	15.60	15.60	15.60	15.60	15.60
2,2	I	15.61	15.61	15.62	15.61	15.62	15.62
4,1	I	20.62	20.65	20.63	20.63	20.62	20.62
3,3	I	21.62	21.62	21.62	21.62	21.62	21.62
4,2	I	22.52	22.55	22.53	22.53	22.52	22.52
2,3	I	24.42	24.42	24.43	24.42	24.43	24.42
4,3	I	26.49	26.51	26.50	26.49	26.49	26.49
$R_\alpha/h = 10$							
1,1	I	20.81	20.82	20.72	20.85	20.82	20.82
0,1	I($w = 0$)	46.99	46.99	47.03	46.99	46.99	46.99
1,2	I	47.28	47.26	47.11	47.64	47.29	47.31
2,1	I	49.51	49.65	49.23	49.52	49.59	49.52
2,2	I	65.53	65.62	65.08	65.82	65.58	65.55
1,3	I	82.06	82.01	81.73	83.31	82.06	82.09
1,0	II($w = 0$)	89.79	89.79	89.80	89.79	89.79	89.85
0,2	I($w = 0$)	93.99	93.99	93.25	93.99	93.98	93.97
2,3	I	93.94	94.00	94.07	95.14	93.99	93.99
3,1	I	100.6	101.1	99.80	100.5	100.9	100.6
$R_\alpha/h = 5$							
1,1	I	32.17	32.22	31.82	32.36	32.20	32.20
0,1	I($w = 0$)	46.99	46.99	47.10	46.99	46.99	46.99
1,2	I	66.12	66.10	65.43	67.31	66.13	66.17
2,1	I	83.55	84.10	82.24	83.47	83.85	83.63
1,0	II($w = 0$)	89.87	89.88	89.82	89.88	89.87	90.14
0,2	I($w = 0$)	93.99	93.99	94.20	93.99	93.99	93.99
2,2	I	102.8	103.2	101.0	103.4	103.0	102.9
1,3	I	106.5	106.5	104.9	108.9	106.6	106.6
2,3	I	132.9	133.3	130.0	134.6	133.1	133.0
0,3	II($w = 0$)	141.0	141.0	141.3	141.0	141.0	141.0

Table 6: Fourth benchmark, simply supported composite cylindrical shell $90°/0°/90°$ with thickness ratios $R_\alpha/h = 1000$, $R_\alpha/h = 100$, $R_\alpha/h = 10$ and $R_\alpha/h = 5$. First ten frequencies in Hz, comparison between the present 3D exact solution and several numerical solutions.

m,n	Mode	3D exact	3D FE	2D FE	GDQ-RM	GDQ-ZZ	GDQ-LW
$R_\alpha/h = 1000$							
3,1	I	3.552	3.560	3.556	3.552	3.552	3.552
4,1	I	4.395	4.429	4.404	4.395	4.396	4.395
2,1	I	5.353	5.354	5.356	5.353	5.353	5.353
5,1	I	6.491	6.578	6.510	6.492	6.492	6.491
4,2	I	6.716	6.738	6.728	6.716	6.716	6.716
5,2	I	7.432	7.508	7.452	7.432	7.432	7.431
3,2	I	8.394	8.397	8.403	8.394	8.394	8.394
6,1	I	9.268	9.449	9.306	9.269	9.269	9.268
5,3	I	9.544	9.603	9.570	9.544	9.544	9.544
6,2	I	9.663	9.837	9.702	9.664	9.664	9.663
$R_\alpha/h = 100$							
2,1	I	11.24	11.25	11.26	11.25	11.25	11.24
1,1	I	13.20	13.20	13.22	13.21	13.20	13.21
2,2	I	17.22	17.23	17.25	17.23	17.22	17.22
3,1	I	22.84	22.85	22.87	22.87	22.84	22.83
3,2	I	24.59	24.61	24.63	24.63	24.59	24.58
2,3	I	24.87	24.87	24.90	24.88	24.87	24.87
3,3	I	28.10	28.07	28.09	28.07	28.07	28.07
1,2	I	28.07	28.12	28.15	28.14	28.10	28.09
2,4	I	33.09	33.09	33.14	33.11	33.09	33.10
3,4	I	33.11	33.13	33.17	33.16	33.12	33.11
$R_\alpha/h = 10$							
1,1	I	25.20	25.31	25.31	25.55	25.22	25.16
1,2	I	43.72	43.76	43.81	44.24	43.75	43.78
0,1	I($w = 0$)	46.99	46.99	47.03	46.99	46.99	46.99
1,3	I	70.66	70.66	70.76	72.02	70.75	70.85
2,1	I	77.58	78.33	77.59	80.67	77.76	77.28
2,2	I	84.74	85.50	84.50	87.77	84.91	84.52
1,0	II($w = 0$)	89.79	89.79	89.79	89.79	89.79	89.86
0,2	I($w = 0$)	93.99	93.99	94.06	93.99	93.99	93.99
2,3	I	100.6	101.3	100.0	103.9	100.8	100.6
1,4	I	102.8	102.8	102.8	105.9	103.0	103.1
$R_\alpha/h = 5$							
1,1	I	38.63	39.05	38.69	40.13	38.70	38.49
0,1	I($w = 0$)	46.99	46.99	47.10	46.99	47.00	46.99
1,2	I	61.81	62.06	61.64	64.00	61.93	62.01
1,0	II($w = 0$)	89.87	89.88	89.82	89.88	89.87	90.16
0,2	I($w = 0$)	93.99	93.99	94.20	93.99	93.99	93.99
1,3	I	95.17	95.25	94.63	99.57	95.42	95.73
2,1	I	107.5	109.0	106.0	114.6	107.9	106.9
2,2	I	117.9	119.3	115.6	124.7	118.2	117.5
1,4	I	132.2	132.2	130.6	139.3	132.6	133.1
2,3	I	138.0	139.2	134.9	141.0	138.4	138.0

Table 7: Fifth benchmark, simply supported composite cylindrical shell 90°/0°/90°/0° with thickness ratios $R_\alpha/h = 1000$, $R_\alpha/h = 100$, $R_\alpha/h = 10$ and $R_\alpha/h = 5$. First ten frequencies in Hz, comparison between the present 3D exact solution and several numerical solutions.

m,n	Mode	3D exact	3D FE	2D FE	GDQ-RM	GDQ-ZZ	GDQ-LW
$R_\alpha/h = 1000$							
3,1	I	3.644	3.645	3.646	3.650	3.644	3.643
4,1	I	5.082	5.087	5.091	5.107	5.084	5.083
2,1	I	5.230	5.231	5.232	5.231	5.230	5.230
4,2	I	7.269	7.272	7.280	7.290	7.270	7.269
5,1	I	7.667	7.676	7.689	7.728	7.670	7.667
5,2	I	8.554	8.562	8.575	8.615	8.557	8.554
3,2	I	9.179	9.179	9.187	9.183	9.179	9.179
6,1	I	10.93	10.95	10.98	11.02	10.94	10.94
5,3	I	10.97	10.97	10.99	11.06	10.97	10.97
6,2	I	11.41	11.43	11.45	11.54	11.42	11.41
$R_\alpha/h = 100$							
2,1	I	12.19	12.19	12.19	13.51	12.25	12.19
1,1	I	16.62	16.62	16.62	16.65	16.62	16.62
2,2	I	21.41	21.41	21.41	22.67	21.47	21.41
3,1	I	22.17	22.18	22.14	27.86	22.38	22.17
3,2	I	25.16	25.16	25.11	31.44	25.38	25.16
3,3	I	31.30	31.31	31.24	35.80	31.54	31.30
2,3	I	34.27	34.27	34.28	38.40	34.33	34.27
4,1	I	34.58	34.59	34.43	40.92	35.02	34.58
4,2	I	36.21	36.22	36.04	47.92	36.68	36.21
4,3	I	39.44	39.45	39.23	48.55	39.78	39.44
$R_\alpha/h = 10$							
1,1	I	20.04	20.04	19.59	35.96	20.05	20.03
2,1	I	29.48	29.48	23.92	68.09	29.56	29.51
2,2	I	37.10	37.10	30.80	78.27	37.18	37.11
1,2	I	43.94	43.94	35.72	107.3	43.95	43.94
2,3	I	49.74	49.74	38.19	111.8	49.84	49.75
3,1	I	52.80	52.81	42.10	131.9	53.01	52.89
3,2	I	57.02	57.04	43.27	149.6	57.26	57.11
1,3	I	61.47	61.47	43.30	153.2	61.49	61.50
2,4	I	63.85	63.86	47.82	156.5	63.99	63.87
3,3	I	64.73	64.74	49.25	164.9	65.00	64.82
$R_\alpha/h = 5$							
1,1	I	21.93	21.93	19.36	60.54	22.11	21.92
2,1	I	42.96	42.97	22.24	78.28	43.53	43.34
1,2	I	46.27	46.27	29.28	103.0	46.45	46.30
2,2	I	52.38	52.39	32.93	149.8	52.96	52.73
1,3	I	66.24	66.23	35.36	156.5	66.48	66.39
2,3	I	68.19	68.20	40.47	159.4	68.81	68.53
0,1	I($w = 0$)	78.29	78.25	40.72	173.7	78.28	78.25
1,4	I	83.21	83.22	43.19	178.5	83.56	83.47
3,1	I	83.84	83.86	43.99	204.1	84.51	84.83
2,4	I	87.74	87.75	45.35	222.7	88.44	88.12

Table 8: Sixth benchmark, simply supported sandwich cylindrical shell embedding isotropic skins and PVC core with thickness ratios $R_\alpha/h = 1000$, $R_\alpha/h = 100$, $R_\alpha/h = 10$ and $R_\alpha/h = 5$. First ten frequencies in Hz, comparison between the present 3D exact solution and several numerical solutions.

m,n	Mode	3D exact	3D FE	2D FE	GDQ-RM	GDQ-ESL	GDQ-LW
$R_\alpha/h = 1000$							
1,1	I	77.54	76.21	76.29	76.30	76.29	76.29
2,1	I	79.76	78.79	78.81	78.83	78.83	78.83
1,2	I	79.76	79.40	79.41	79.42	79.42	79.42
2,2	I	80.33	79.93	79.97	79.98	79.98	79.98
3,1	I	80.53	80.01	80.00	80.02	80.02	80.02
3,2	I	80.73	80.41	80.45	80.44	80.44	80.44
4,1	I	80.90	80.59	80.50	80.51	80.51	80.51
2,3	I	80.73	80.61	80.60	80.59	80.59	80.59
3,3	I	80.94	80.75	80.63	80.61	80.61	80.61
4,2	I	81.00	80.76	80.81	80.81	80.80	80.80
$R_\alpha/h = 100$							
1,1	I	77.63	76.75	76.81	76.82	76.80	76.80
2,1	I	80.42	79.59	79.62	79.64	79.63	79.63
1,2	I	80.42	80.51	80.54	80.55	80.54	80.54
2,2	I	82.09	82.05	82.13	82.14	82.12	82.12
3,1	I	83.29	82.94	82.96	82.98	82.96	82.96
1,3	I	83.29	83.95	84.00	84.02	83.99	83.99
3,2	I	85.40	85.64	85.71	85.72	85.69	85.69
2,3	I	85.40	85.72	85.80	85.82	85.78	85.78
4,1	I	88.80	88.96	88.96	88.98	88.94	88.94
1,4	I	88.80	89.05	89.06	89.07	89.04	89.04
$R_\alpha/h = 10$							
1,1	I	85.70	84.98	85.32	85.45	85.17	85.17
2,1	I	125.3	125.7	125.9	126.1	125.8	125.8
1,2	I	125.3	125.7	125.9	126.2	125.8	125.8
0,1	II($w = 0$)	150.9	137.6	138.3	138.0	138.0	138.0
1,0	II($w = 0$)	150.9	158.7	159.5	159.1	159.1	159.1
2,2	I	172.5	176.5	176.4	176.7	176.7	176.7
1,3	I	204.4	205.2	204.7	205.2	205.5	205.5
3,1	I	204.4	207.9	207.2	207.7	208.0	208.0
1,1	II($w = 0$)	213.4	226.4	226.9	226.4	226.4	226.4
2,3	I	251.6	256.3	255.2	255.9	256.7	256.7
$R_\alpha/h = 5$							
1,1	I	103.1	102.1	102.4	102.9	102.3	102.3
0,1	II($w = 0$)	149.9	136.6	138.3	137.1	137.1	137.1
1,0	II($w = 0$)	149.9	156.7	158.3	157.0	157.1	157.1
2,1	I	183.8	185.1	184.0	184.8	185.3	185.3
1,2	I	183.8	185.3	184.8	185.4	185.8	185.8
1,1	II($w = 0$)	212.0	224.6	226.6	224.6	224.6	224.6
2,2	I	259.6	265.3	262.9	263.8	265.9	265.9
0,2	II($w = 0$)	299.6	292.7	296.3	293.6	293.6	293.6
1,3	I	305.6	306.0	302.8	304.1	307.2	307.2
3,1	I	305.6	310.7	306.2	307.6	310.8	310.8

Table 9: Seventh benchmark, simply supported spherical shell made of aluminium alloy with thickness ratios $R_\alpha/h = 1000$, $R_\alpha/h = 100$, $R_\alpha/h = 10$ and $R_\alpha/h = 5$. First ten frequencies in Hz, comparison between the present 3D exact solution and several numerical solutions.

m,n	Mode	3D exact	3D FE	2D FE	GDQ-RM	GDQ-ZZ	GDQ-LW
			$R_\alpha/h = 1000$				
1,1	I	88.00	86.60	89.95	86.59	86.58	86.58
2,1	I	90.52	89.46	92.31	89.46	89.46	89.45
1,2	I	90.52	90.14	92.98	90.13	90.13	90.13
2,2	I	91.17	90.77	93.26	90.76	90.76	90.76
3,1	I	91.39	90.81	93.73	90.81	90.81	90.80
3,2	I	91.61	91.30	93.75	91.29	91.29	91.28
2,3	I	91.61	91.42	94.08	91.36	91.36	91.35
4,1	I	91.81	91.48	94.12	91.46	91.46	91.45
3,3	I	91.85	91.65	94.18	91.49	91.48	91.48
4,2	I	91.92	91.71	94.54	91.70	91.70	91.69
			$R_\alpha/h = 100$				
1,1	I	88.04	87.03	90.58	87.12	87.09	87.04
2,1	I	91.17	90.23	93.19	90.30	90.27	90.22
1,2	I	91.17	91.27	94.43	91.33	91.30	91.25
2,2	I	93.02	92.97	96.46	93.08	93.04	92.99
3,1	I	94.34	93.94	96.57	93.99	93.95	93.91
1,3	I	94.34	95.09	97.86	95.18	95.13	95.08
3,2	I	96.65	96.91	100.1	97.01	96.96	96.92
2,3	I	96.65	97.01	100.4	97.12	97.08	97.03
4,1	I	100.4	100.5	102.8	100.6	100.5	100.5
1,4	I	100.4	100.7	103.3	100.7	100.6	100.6
			$R_\alpha/h = 10$				
1,1	I	96.20	95.40	101.0	95.99	95.61	95.31
2,1	I	139.4	139.9	150.0	140.4	140.0	140.0
1,2	I	139.4	139.9	150.2	140.5	140.1	140.1
0,1	II($w = 0$)	172.2	157.0	164.7	157.5	157.5	156.8
1,0	II($w = 0$)	172.2	181.1	189.9	181.6	181.6	180.8
2,2	I	191.3	195.7	216.1	196.2	196.0	196.3
1,3	I	226.6	227.5	254.2	227.8	227.7	228.1
3,1	I	226.6	230.4	257.9	230.4	230.5	230.9
1,1	II($w = 0$)	243.5	258.4	264.5	258.4	258.4	257.2
2,3	I	278.6	283.9	325.9	284.0	284.3	284.9
			$R_\alpha/h = 5$				
1,1	I	114.4	113.3	125.2	114.3	113.5	113.5
0,1	II($w = 0$)	172.1	156.9	164.6	157.4	157.4	156.4
1,0	II($w = 0$)	172.1	179.7	189.0	180.0	180.1	179.1
2,1	I	202.6	204.0	245.4	204.3	204.2	205.0
1,2	I	202.6	204.6	245.9	205.3	205.1	205.8
1,1	II($w = 0$)	243.4	257.9	263.7	257.9	257.9	256.3
2,2	I	286.0	292.5	353.3	292.3	293.1	294.5
0,2	II($w = 0$)	344.1	336.2	373.8	337.2	337.1	335.0
1,3	I	337.0	337.8	376.2	337.4	338.8	340.4
3,1	I	337.0	342.7	400.1	341.2	342.8	344.5

Table 10: Eighth benchmark, simply supported spherical shell made of aluminium alloy and titanium alloy with thickness ratios $R_\alpha/h = 1000$, $R_\alpha/h = 100$, $R_\alpha/h = 10$ and $R_\alpha/h = 5$. First ten frequencies in Hz, comparison between the present 3D exact solution and several numerical solutions.

m,n	Mode	3D exact	3D FE	2D FE	GDQ-RM	GDQ-ZZ	GDQ-LW
$R_\alpha/h = 1000$							
1,1	I	82.59	81.28	84.43	81.27	81.26	81.26
2,1	I	84.96	83.96	86.64	83.96	83.96	83.96
1,2	I	84.96	84.60	87.27	84.59	84.59	84.59
2,2	I	85.57	85.19	87.54	85.18	85.18	85.18
3,1	I	85.78	85.23	87.97	85.23	85.23	85.23
3,2	I	85.98	85.68	87.99	85.68	85.68	85.68
2,3	I	85.98	85.78	88.30	85.74	85.74	85.74
4,1	I	86.16	85.87	88.32	85.83	85.83	85.84
3,3	I	86.20	85.89	88.39	85.86	85.86	85.86
4,2	I	86.27	86.07	88.72	86.06	86.06	86.06
$R_\alpha/h = 100$							
1,1	I	82.60	81.71	85.06	81.71	81.70	81.71
2,1	I	85.51	84.66	87.48	84.67	84.66	84.67
1,2	I	85.51	85.63	88.63	85.63	85.62	85.63
2,2	I	87.17	87.19	90.40	87.20	87.18	87.20
3,1	I	88.35	87.98	90.51	87.99	87.97	87.99
1,3	I	88.35	89.11	91.72	89.12	89.09	89.11
3,2	I	90.39	90.67	93.62	90.68	90.66	90.68
2,3	I	90.39	90.80	93.88	90.80	90.78	90.80
4,1	I	93.69	93.83	96.02	93.83	93.80	93.84
1,4	I	93.69	93.98	96.48	93.97	93.95	93.98
$R_\alpha/h = 10$							
1,1	I	89.41	88.88	95.25	89.06	88.88	89.29
2,1	I	127.8	128.3	140.1	128.5	128.3	129.6
1,2	I	127.8	128.4	140.3	128.7	128.5	129.7
0,1	II($w = 0$)	158.6	145.0	154.5	145.0	145.0	145.4
1,0	II($w = 0$)	158.6	167.2	178.2	167.2	167.2	167.6
2,2	I	174.1	178.4	200.7	178.8	178.6	180.7
1,3	I	205.7	206.8	236.1	207.3	207.2	209.6
3,1	I	205.7	209.2	239.3	209.7	209.6	212.1
1,1	II($w = 0$)	224.3	237.9	248.0	237.9	237.9	238.5
2,3	I	252.5	257.6	301.6	258.4	258.1	261.2
$R_\alpha/h = 5$							
1,1	I	104.8	103.8	118.8	104.4	104.1	105.9
0,1	II($w = 0$)	155.5	141.8	154.4	142.3	142.3	143.3
1,0	II($w = 0$)	155.5	162.4	177.3	162.7	162.7	164.0
2,1	I	182.7	183.9	231.0	184.9	184.6	189.2
1,2	I	182.7	184.5	231.4	185.8	185.4	189.9
1,1	II($w = 0$)	219.9	233.0	247.5	233.0	233.0	234.7
2,2	I	256.5	262.2	331.4	264.6	263.7	270.4
1,3	I	301.4	302.0	350.3	304.6	304.2	306.7
0,2	II($w = 0$)	310.7	303.6	352.3	305.7	304.5	311.8
3,1	I	301.4	306.3	375.5	309.2	307.7	315.5

Table 11: Ninth benchmark, simply supported spherical shell made of aluminium alloy, titanium alloy and steel with thickness ratios $R_\alpha/h = 1000$, $R_\alpha/h = 100$, $R_\alpha/h = 10$ and $R_\alpha/h = 5$. First ten frequencies in Hz, comparison between the present 3D exact solution and several numerical solutions.

m,n	Mode	3D exact	3D FE	2D FE	GDQ-RM	GDQ-ZZ	GDQ-LW
			$R_\alpha/h = 1000$				
1,1	I	51.30	51.22	53.10	51.17	51.16	51.16
2,2	I	54.35	54.50	56.65	54.49	54.49	54.49
3,3	I	55.06	55.23	57.44	55.22	55.21	55.21
4,4	I	55.57	55.74	58.02	55.73	55.73	55.73
3,4	I	56.33	55.98	58.83	55.97	55.97	55.97
4,5	I	56.55	56.31	59.08	56.30	56.30	56.30
2,3	I	56.94	56.37	59.31	56.36	56.36	56.36
5,5	I	56.26	56.46	59.40	56.44	56.44	56.44
5,6	I	57.39	57.20	59.45	57.17	57.17	57.17
6,6	I	57.39	57.63	59.95	57.58	57.58	57.58
			$R_\alpha/h = 100$				
1,1	I	51.41	51.60	53.36	51.56	51.54	51.55
2,2	I	56.68	56.91	59.26	56.94	56.92	56.92
1,2	I	61.71	60.55	63.71	60.59	60.57	60.58
3,2	I	62.28	63.33	65.04	63.35	63.33	63.35
2,3	I	66.18	64.50	65.42	64.54	64.51	64.52
3,3	I	66.36	66.74	69.96	66.79	66.75	66.75
2,1	I	64.01	66.75	70.02	66.82	66.76	66.77
4,3	I	71.64	72.88	73.32	72.95	72.89	72.90
4,2	I	71.38	73.10	75.56	73.12	73.09	73.10
1,3	I	76.60	75.91	79.87	76.06	76.00	76.01
			$R_\alpha/h = 10$				
1,1	I	60.00	60.01	63.57	60.53	60.15	60.26
0,1	I	88.90	81.92	86.16	81.92	81.92	82.04
2,1	I	85.73	87.23	90.90	87.69	87.23	87.38
1,0	I($w = 0$)	89.56	94.98	101.3	94.68	94.64	94.78
1,2	I	116.1	115.3	144.8	118.5	116.0	116.2
2,2	I	127.9	129.1	156.0	131.7	129.3	129.7
3,1	I	130.4	133.7	176.6	133.9	133.5	133.5
3,2	I	160.9	165.8	184.9	167.4	165.8	166.0
0,2	II($w = 0$)	179.1	175.5	197.7	175.5	175.5	176.0
2,0	II($w = 0$)	179.1	187.8	216.1	187.6	187.6	188.0
			$R_\alpha/h = 5$				
1,1	I	71.50	71.04	85.94	72.45	71.29	71.81
0,1	I($w = 0$)	88.99	81.40	86.17	81.39	81.39	81.87
1,0	I($w = 0$)	88.99	94.75	100.4	94.28	94.23	94.78
2,1	I	112.4	114.4	139.6	115.0	114.3	114.9
1,2	I	141.5	140.7	184.9	144.2	141.2	142.2
2,2	I	164.3	166.8	197.7	168.7	166.8	167.9
0,2	II($w = 0$)	177.8	174.3	234.8	174.2	174.2	175.3
3,1	I	176.1	180.9	273.2	179.9	180.4	180.6
2,0	II($w = 0$)	177.8	186.5	280.6	186.3	186.3	187.3
3,2	I	212.3	219.6	296.1	219.2	219.2	220.1

Table 12: Tenth benchmark, simply supported composite spherical shell $90°/0°/90°$ with thickness ratios $R_\alpha/h = 1000$, $R_\alpha/h = 100$, $R_\alpha/h = 10$ and $R_\alpha/h = 5$. First ten frequencies in Hz, comparison between the present 3D exact solution and several numerical solutions.

m,n	Mode	3D exact	3D FE	2D FE	GDQ-RM	GDQ-ZZ	GDQ-LW
$R_\alpha/h = 1000$							
1,1	I	51.52	51.30	53.54	51.23	51.20	51.22
2,2	I	54.64	54.68	57.11	54.66	54.66	54.66
3,3	I	55.35	55.41	57.90	55.40	55.39	55.40
4,4	I	55.83	55.91	58.44	55.89	55.89	55.89
5,5	I	56.45	56.60	59.14	56.57	56.57	56.57
3,4	I	57.25	56.74	59.31	56.73	56.73	56.73
4,5	I	57.14	56.77	59.37	56.76	56.76	56.76
5,6	I	57.62	57.32	59.87	57.29	57.28	57.28
2,3	I	58.28	57.50	60.04	57.50	57.50	57.50
6,6	I	57.45	57.70	60.23	57.64	57.64	57.64
$R_\alpha/h = 100$							
1,1	I	51.62	51.58	53.80	51.53	51.51	51.51
2,2	I	56.69	56.85	59.26	56.86	56.84	56.85
1,2	I	63.26	61.73	64.32	61.76	61.75	61.74
2,3	I	63.97	62.86	65.39	62.89	62.86	62.87
2,1	I	63.17	64.96	67.26	64.94	64.91	64.93
3,2	I	63.79	65.05	67.44	65.06	65.03	65.03
3,3	I	65.43	66.21	68.56	66.24	66.19	66.20
3,4	I	75.97	76.58	79.02	76.66	76.56	76.57
2,4	I	77.62	76.91	79.47	77.02	76.94	76.95
1,3	I	78.12	76.96	79.52	77.05	77.01	76.99
$R_\alpha/h = 10$							
1,1	I	59.61	59.26	62.47	59.49	59.13	59.27
0,1	I($w = 0$)	89.56	81.92	86.16	81.92	81.92	82.04
1,0	I($w = 0$)	89.56	94.86	100.0	94.72	94.56	94.71
1,2	I	102.9	103.0	120.0	105.2	102.8	102.4
2,1	I	101.3	103.5	122.0	105.6	103.2	103.6
2,2	I	128.1	131.9	163.5	135.0	131.1	131.2
1,3	I	168.2	167.5	184.9	175.3	168.1	167.1
3,1	I	164.9	170.0	197.6	175.5	168.3	169.0
0,2	II($w = 0$)	179.1	175.5	232.7	175.6	175.5	175.8
2,3	I	184.1	187.1	238.2	187.7	186.9	187.5
$R_\alpha/h = 5$							
1,1	I	71.66	71.31	82.65	72.55	70.91	71.42
0,1	I($w = 0$)	88.99	81.40	86.17	81.39	81.39	81.90
1,0	I($w = 0$)	88.99	95.13	100.3	94.61	94.61	95.13
1,2	I	130.5	130.3	184.9	135.8	130.1	129.5
2,1	I	128.4	131.5	196.2	136.3	130.5	132.2
2,2	I	166.7	171.0	197.6	174.2	170.3	171.1
0,2	II($w = 0$)	177.8	174.3	208.3	177.9	174.2	175.3
2,0	II($w = 0$)	177.8	186.5	280.6	186.3	186.3	187.4
1,3	I	203.3	203.0	284.7	212.7	203.6	202.5
3,1	I	200.1	205.8	296.2	213.2	204.0	206.6

Table 13: Eleventh benchmark, simply supported composite spherical shell 90°/0°/90°/0° with thickness ratios $R_\alpha/h = 1000$, $R_\alpha/h = 100$, $R_\alpha/h = 10$ and $R_\alpha/h = 5$. First ten frequencies in Hz, comparison between the present 3D exact solution and several numerical solutions.

m,n	Mode	3D exact	3D FE	2D FE	GDQ-RM	GDQ-ZZ	GDQ-LW
$R_\alpha/h = 1000$							
1,1	I	76.66	75.46	78.38	75.46	75.46	75.46
2,1	I	78.86	77.95	80.42	77.95	77.95	77.95
1,2	I	78.86	78.57	81.04	78.56	78.56	78.56
2,2	I	79.44	79.12	81.27	79.12	79.11	79.11
1,3	I	79.65	79.15	81.73	79.14	79.14	79.14
3,2	I	79.86	79.60	81.80	79.60	79.60	79.60
1,5	I	80.43	79.73	82.10	79.71	79.70	79.70
4,1	I	80.06	79.77	82.17	79.77	79.76	79.76
2,3	I	79.86	79.84	82.20	79.81	79.80	79.80
4,2	I	80.19	80.02	82.43	80.02	80.02	80.02
$R_\alpha/h = 100$							
1,1	I	76.81	76.02	79.07	76.15	76.00	76.00
2,1	I	79.83	79.05	81.82	79.41	79.05	79.05
1,2	I	79.83	79.94	82.94	80.32	79.93	79.93
2,2	I	81.67	81.71	85.96	82.98	81.70	81.70
3,1	I	82.88	82.55	86.77	84.73	82.55	82.55
1,3	I	82.88	83.53	87.81	85.57	83.51	83.52
3,2	I	84.77	84.98	92.03	89.25	84.98	84.98
2,3	I	84.77	85.11	92.05	89.39	85.10	85.10
4,1	I	87.40	87.43	97.05	94.95	87.42	87.42
1,4	I	87.40	87.62	97.09	95.21	87.60	87.61
$R_\alpha/h = 10$							
1,1	I	78.27	77.73	94.82	90.94	77.75	77.98
2,1	I	85.06	84.48	143.5	136.2	84.52	84.74
1,2	I	85.06	85.27	160.9	148.4	85.31	85.53
2,2	I	91.83	92.41	164.7	150.1	92.51	92.70
3,1	I	96.89	97.13	169.3	158.5	97.27	97.45
1,3	I	96.89	97.44	229.7	215.1	97.57	97.75
2,3	I	105.2	106.3	250.8	223.0	106.5	106.7
3,2	I	105.2	107.0	299.8	250.1	107.3	107.4
1,4	I	117.5	117.8	303.6	252.8	118.1	118.2
4,1	I	117.5	118.8	307.9	291.7	119.1	119.3
$R_\alpha/h = 5$							
1,1	I	79.02	78.56	128.2	115.6	78.65	79.56
2,1	I	91.14	90.79	143.5	134.5	91.13	92.15
1,2	I	91.14	91.43	164.9	154.3	91.76	92.79
2,2	I	105.6	107.0	229.8	214.6	107.7	108.8
1,3	I	116.2	116.8	280.6	214.6	117.8	118.8
3,1	I	116.2	117.2	281.0	220.2	118.2	119.2
1,0	II	123.5	128.1	308.0	287.5	129.6	127.2
0,1	II	123.5	129.5	326.4	300.3	129.7	129.9
2,1	II	134.3	133.9	348.6	305.1	136.0	132.8
1,2	II	134.3	134.2	374.0	330.7	136.7	133.1

Table 14: Twelfth benchmark, simply supported sandwich spherical shell embedding isotropic skins and PVC core with thickness ratios $R_\alpha/h = 1000$, $R_\alpha/h = 100$, $R_\alpha/h = 10$ and $R_\alpha/h = 5$. First ten frequencies in Hz, comparison between the present 3D exact solution and several numerical solutions.

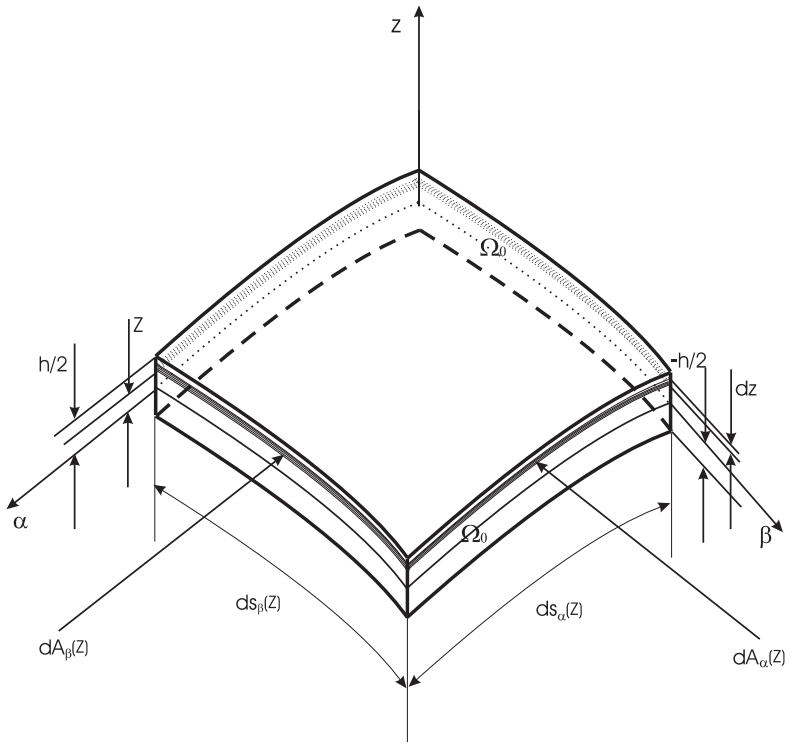

Figure 1: Geometry, notation and reference system for shells.

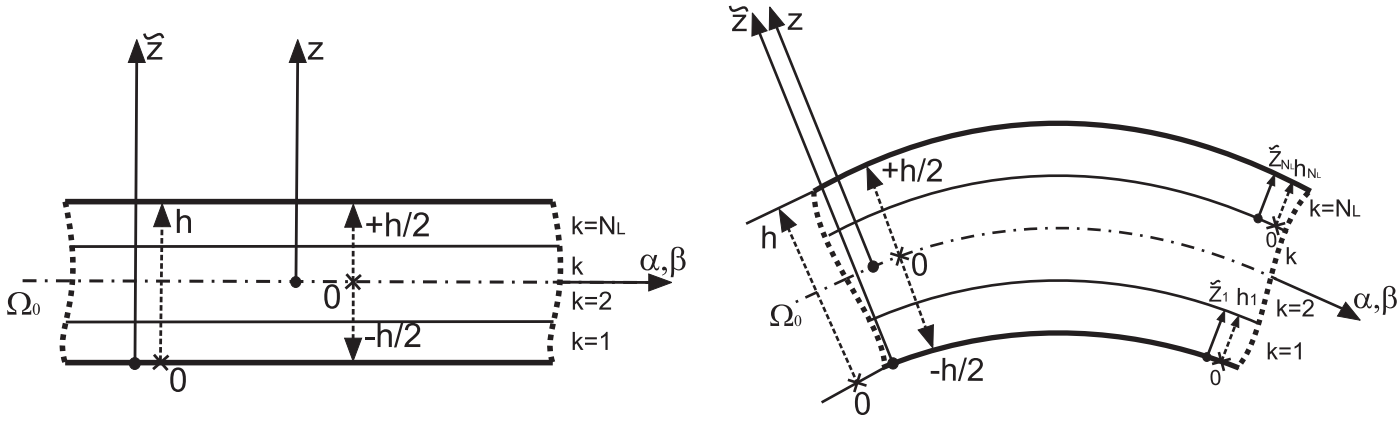

Figure 2: Thickness coordinates and reference systems for plates and shells.

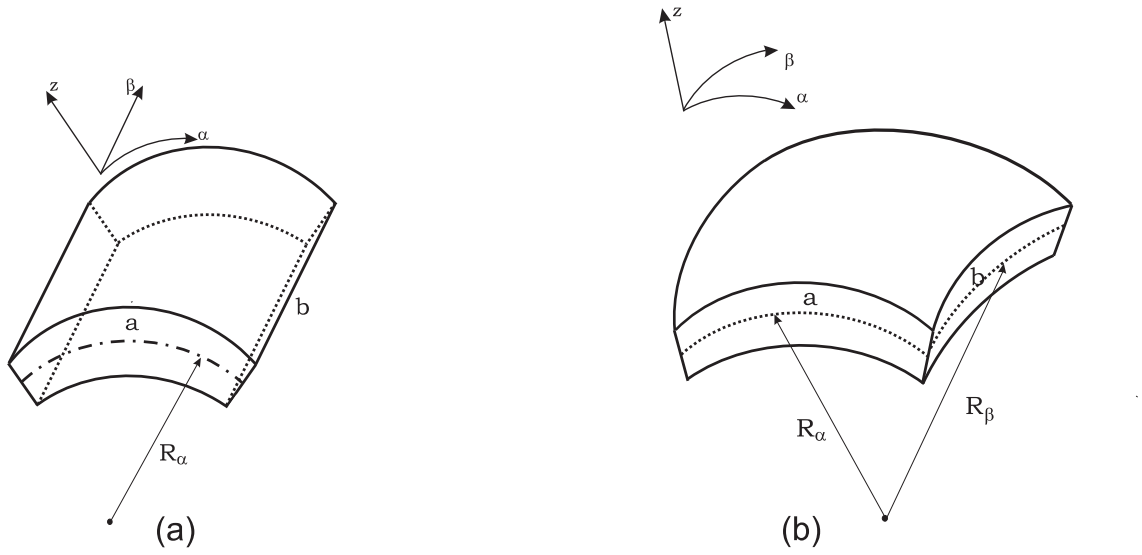

Figure 3: Geometries for the proposed benchmarks: a) cylindrical shell, b) spherical shell.

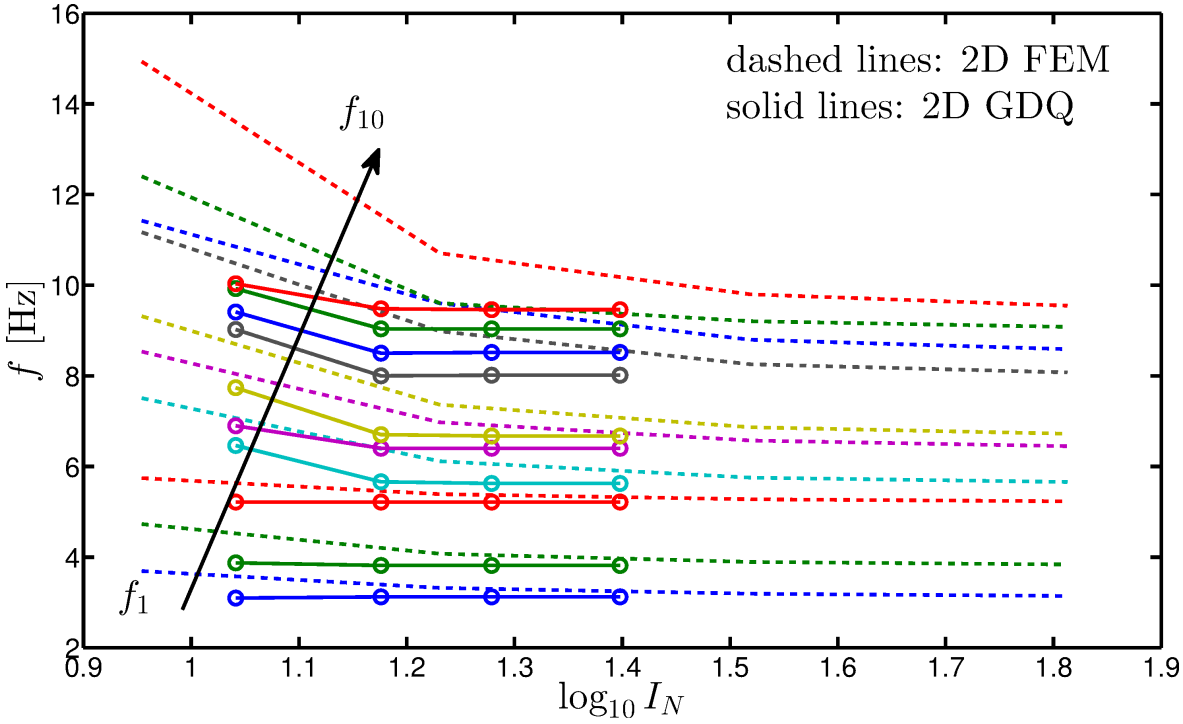

(a)

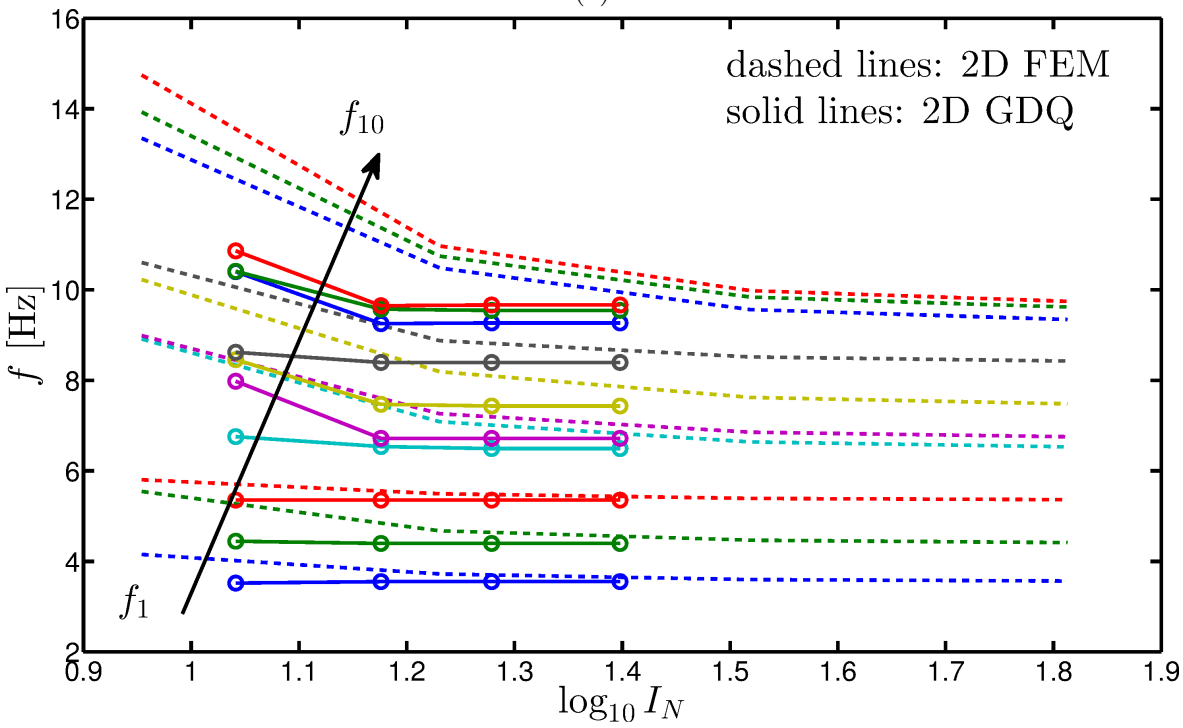

(b)

Figure 4: Convergence of the first ten natural frequencies for a simply-supported cylindrical panel using FE and GDQ methods based on the Reissner-Mindlin model: a) isotropic material, b) laminated $90°/0°/90°/0°$ composite material.

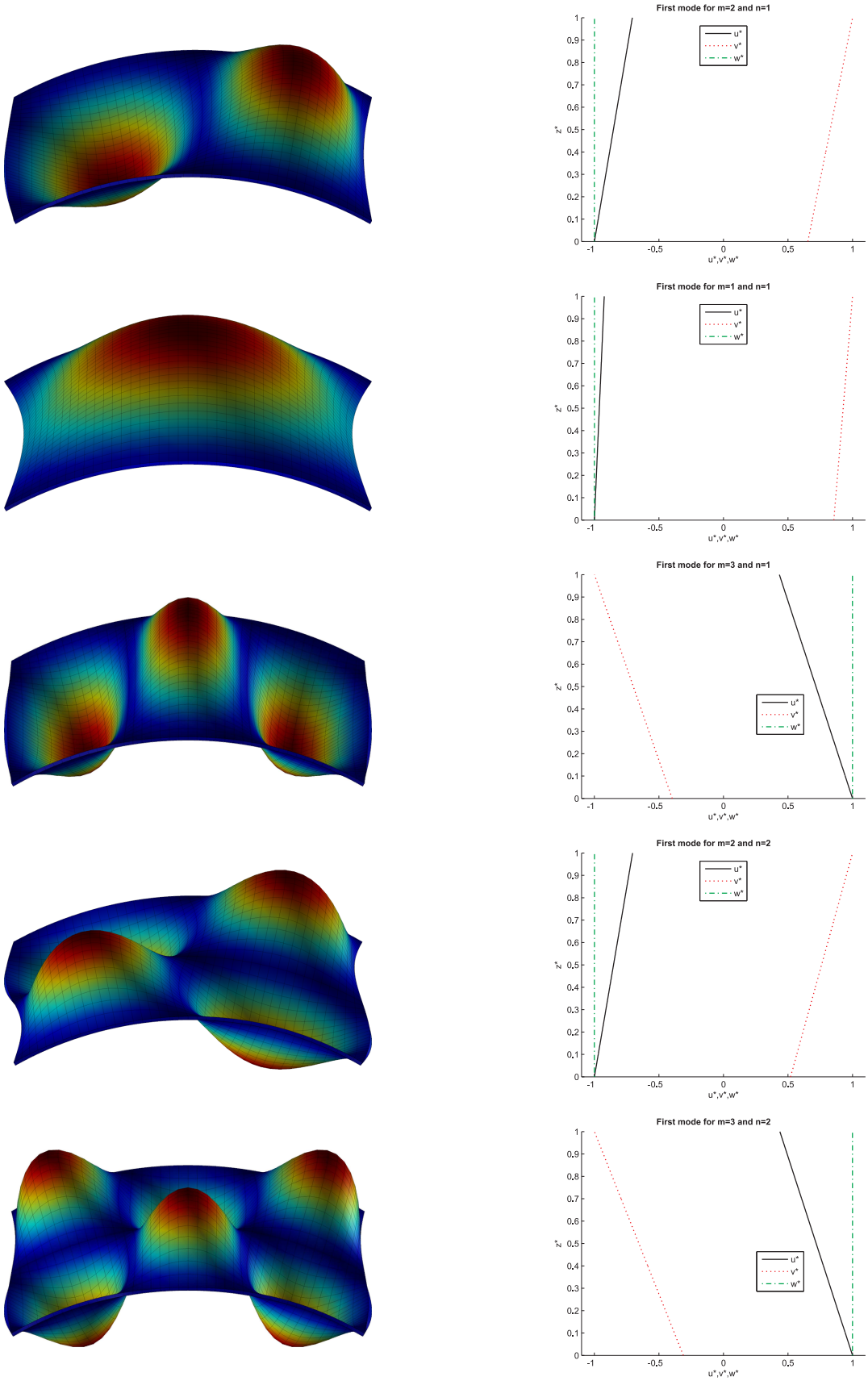

Figure 5: First benchmark, simply supported cylindrical shell made of aluminium alloy with thickness ratio $R_\alpha/h = 100$. First five frequencies via the 2D GDQ solution (on the left) and via the 3D exact solution (on the right).

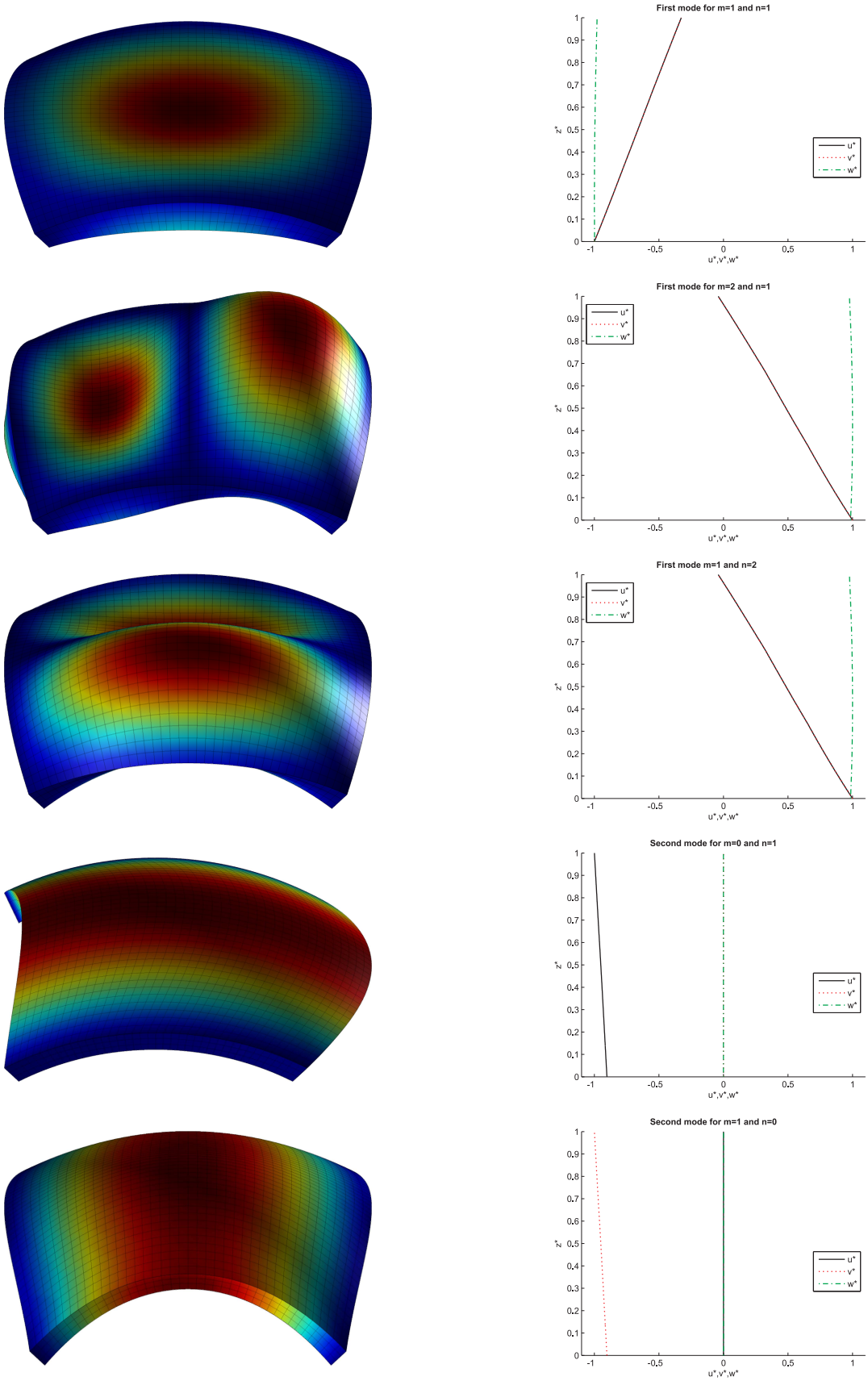

Figure 6: Ninth benchmark, simply supported spherical shell made of aluminium alloy, titanium alloy and steel with thickness ratio $R_\alpha/h = 10$. First five frequencies via the 2D GDQ solution (on the left) and via the 3D exact solution (on the right).

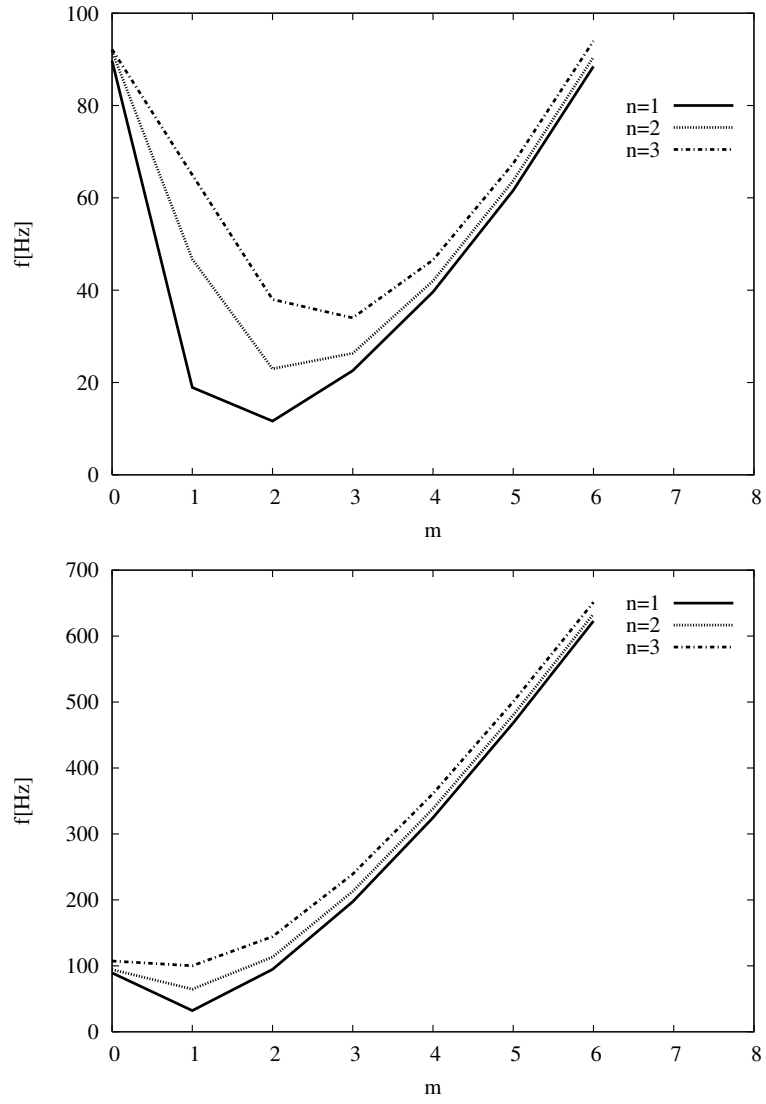

Figure 7: Second benchmark, simply supported cylindrical shell made of aluminium alloy and titanium alloy with thickness ratios R_α/h=100 (top) and R_α/h=10 (bottom). First (I) 3D frequencies versus half-wave numbers m (from 0 to 6) and n (from 1 to 3).

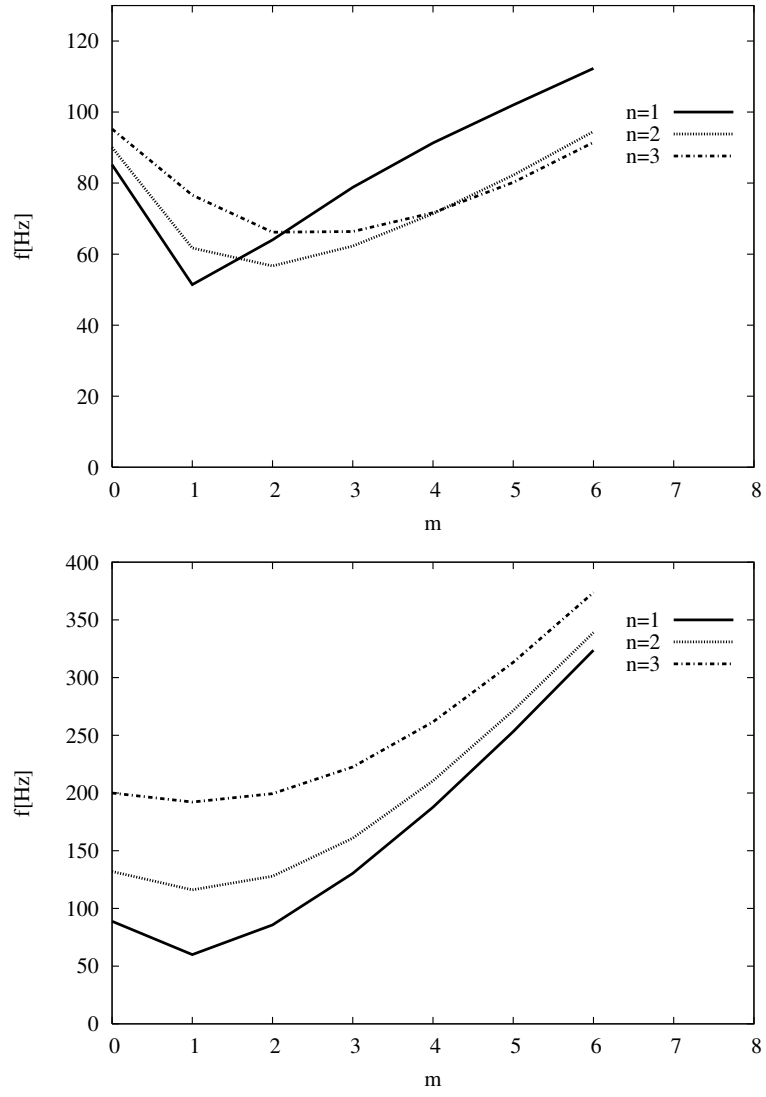

Figure 8: Tenth benchmark, simply supported composite spherical shell 90°/0°/90° with thickness ratios R_α/h=100 (top) and R_α/h=10 (bottom). First (I) 3D frequencies versus half-wave numbers m (from 0 to 6) and n (from 1 to 3).